A review of dynamo experiments

A. Tilgner University of Göttingen

Lehnert (1957)	"blender flow"
Lowes & Wilkinson (1963)	rotating ferromagnetic cylinders
Steenbeck, Kirko, Gailitis (1967)	demonstration of the "α-effect"
Gans (1971)	precessing cylinder
Gailitis et al. (1987)	helical flow with return flow (Ponomarenko)

The induction equation

$$\frac{\partial \vec{B}}{\partial t} + \nabla \times (\vec{B} \times \vec{v}) = \frac{1}{\mu\sigma} \nabla^2 \vec{B}$$

non-dimensional form:

$$\frac{\partial \vec{B}}{\partial t} + \nabla \times (\vec{B} \times \vec{v}) = \frac{1}{R_m} \nabla^2 \vec{B}$$

magnetic Reynolds number $R_m = V \cdot L \cdot \mu\sigma$

$\vec{v} = 0$: pure diffusion

$\vec{v} \neq 0$, $R_m \to \infty$: stretching of $\vec{B}$-field

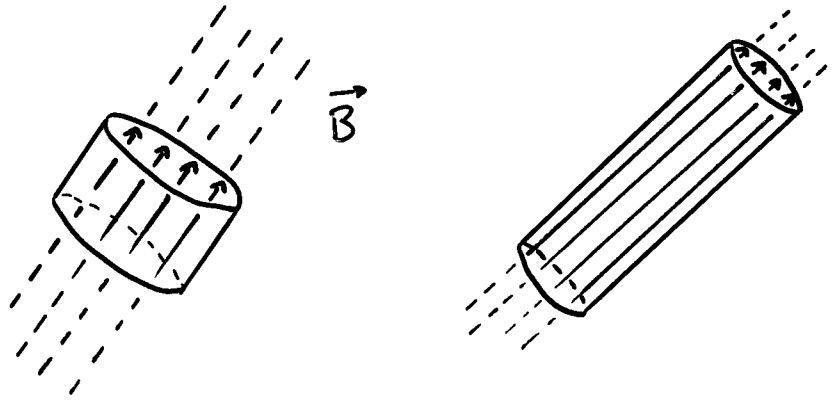

$R_m > 1 - 10$ implies $Re > 10^5 - 10^6$

for liquid metals

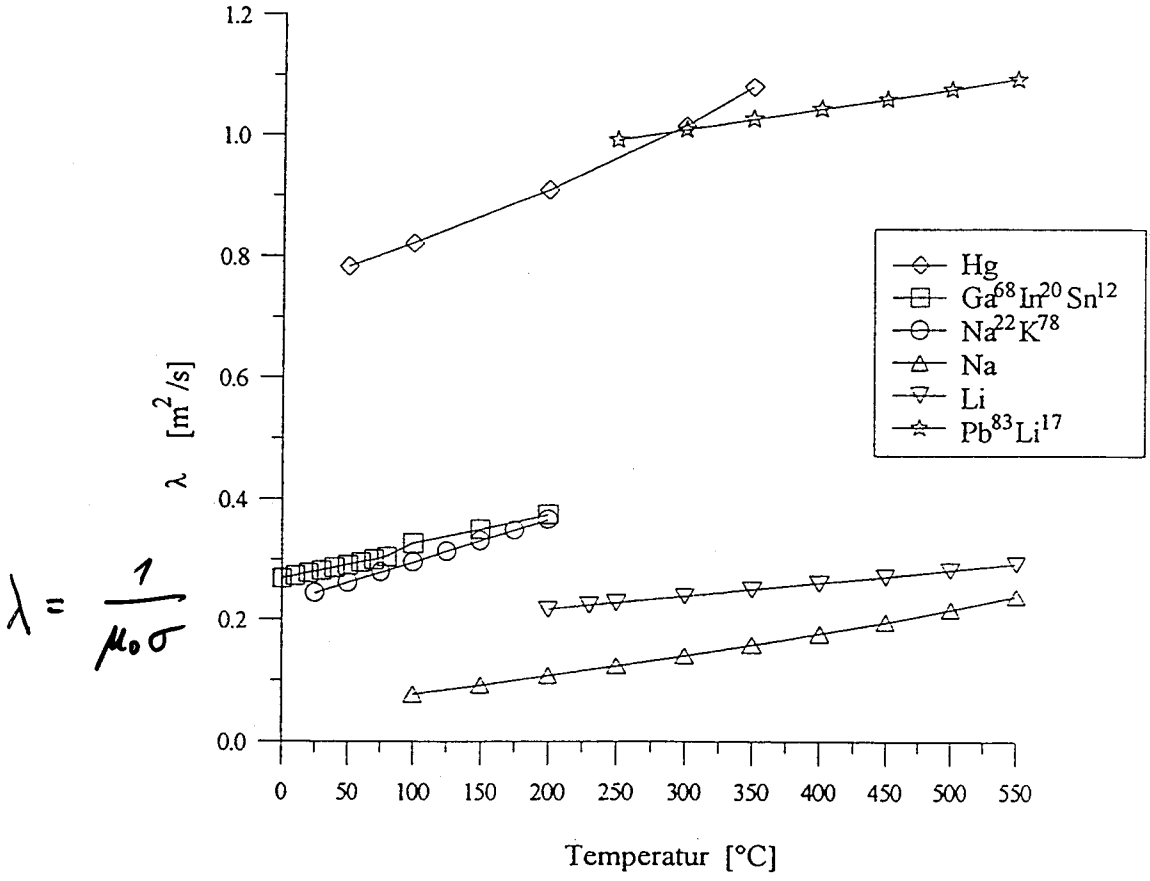

$$\lambda = \frac{1}{\mu_0 \sigma}$$

characteristic size : 1m

$\lambda = 0.1 \ m^2/s$

$Rm = 10 \rightarrow V = 1 \ \frac{m}{s}$

$Rm = 100 \rightarrow V = 10 \ \frac{m}{s}$

Non-rotating convection in Hg:
(Takeshita et al., Cioni et al.)

$Re = 10^6 - 10^7 \rightarrow Ra \approx 10^{12}$

Highest Ra ever reached in Hg: $10^9 - 10^{10}$

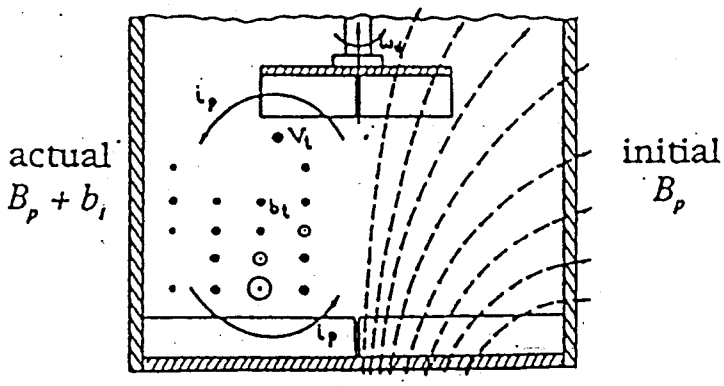

Lehnert (1957)

60 l tank

filled with Na

Gans (1971)

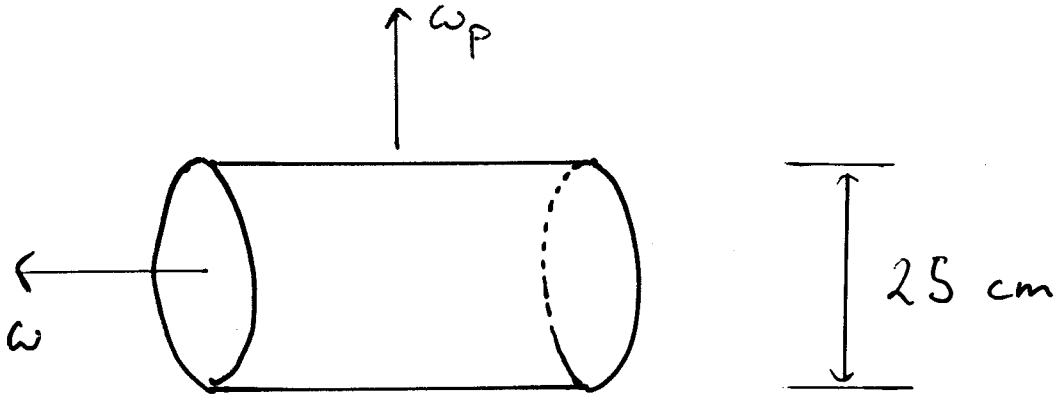

Lowes & Wilkinson (1963)

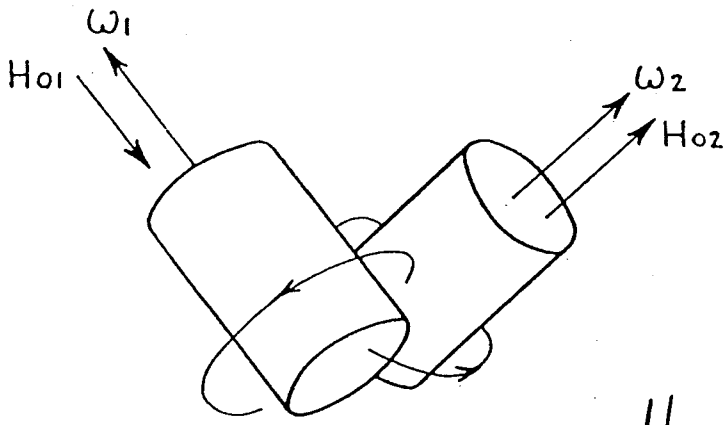

Hg lubricant

ferromagnetic material

$$R_m = V \cdot L \cdot \mu_0 \sigma \cdot \mu$$

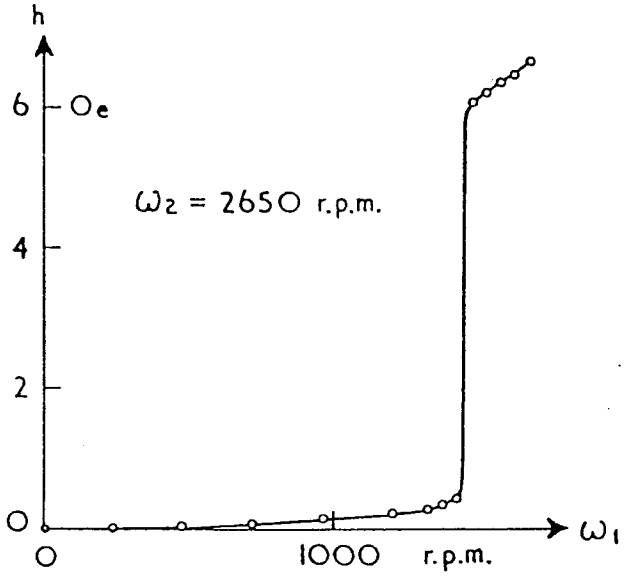

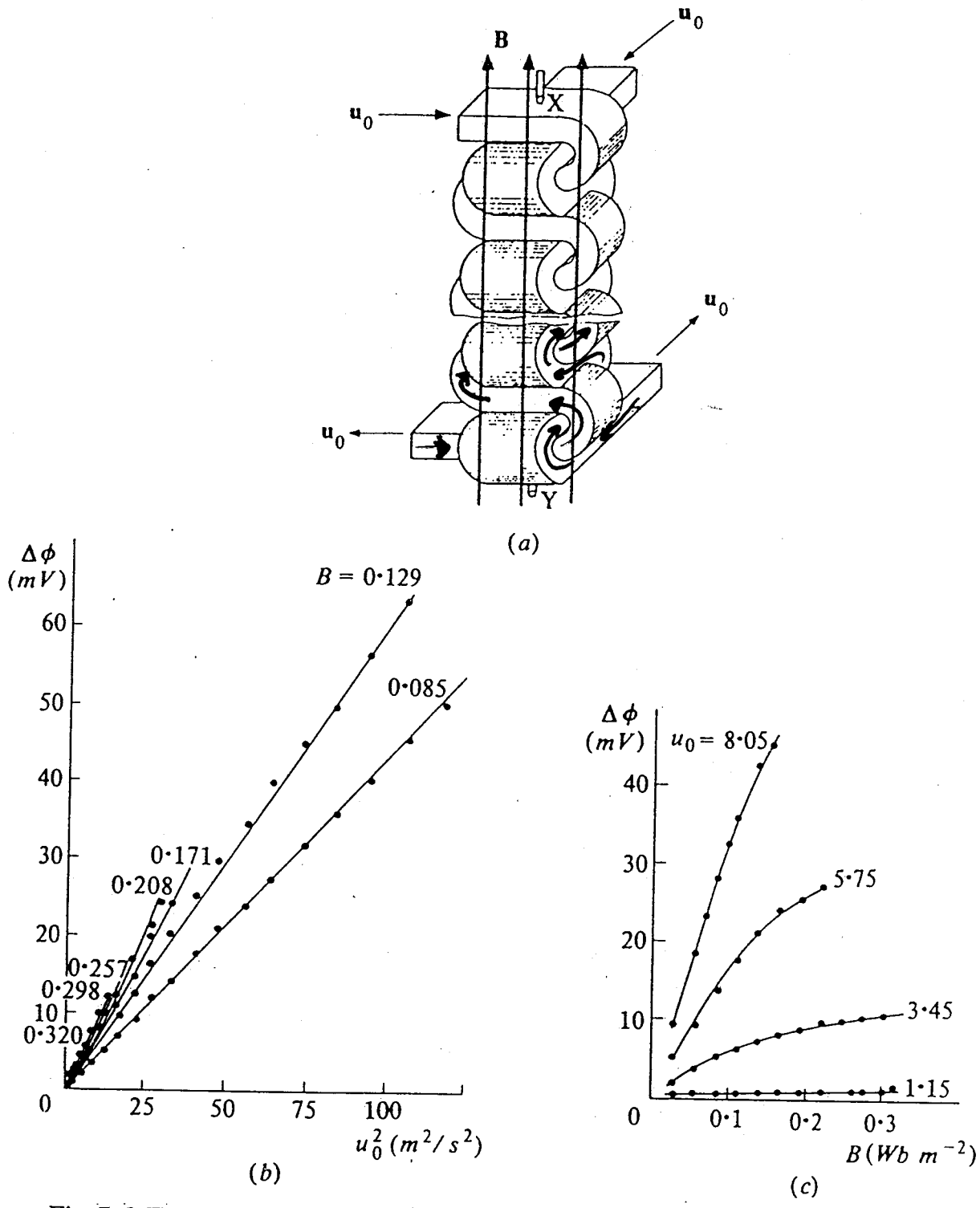

Fig. 7.3 Experimental verification of the α-effect. (*a*) Duct configuration; (*b*) potential difference $\Delta\phi$ measured between the electrodes X and Y as a function of u_0^2 for various values of the applied field **B**; (*c*) $\Delta\phi$ as a function of B for various values of u_0. (Steenbeck *et al.*, 1967.)

Riga

Karlsruhe

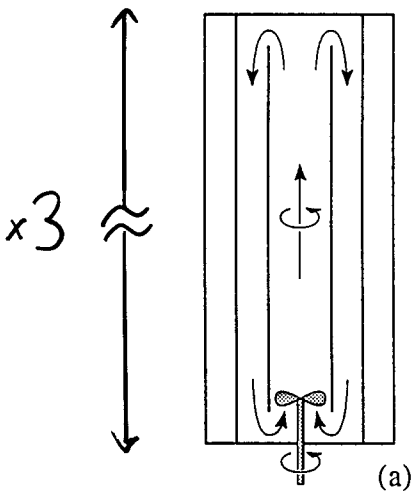

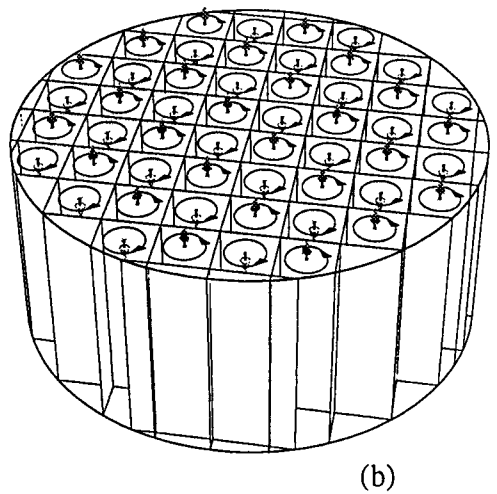

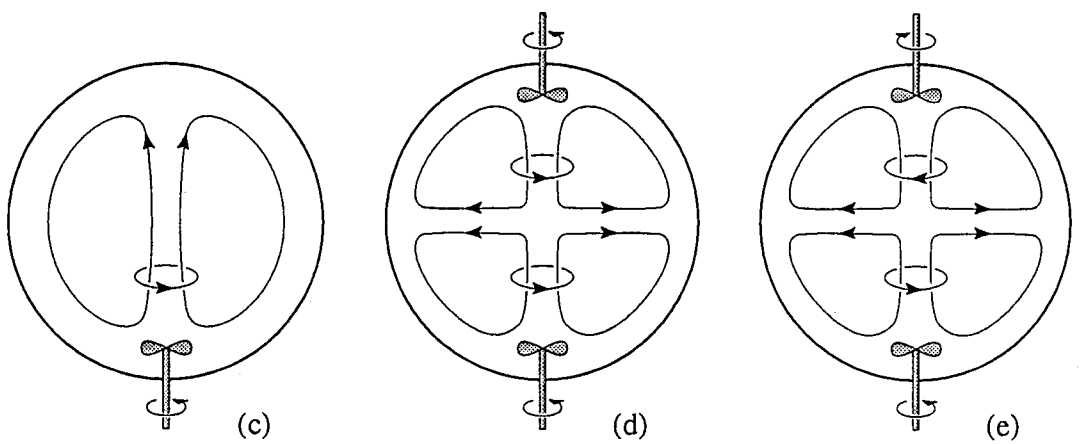

Maryland
Cadarache
Madison

The Ponomarenko Dynamo

Gailitis et al (1987)

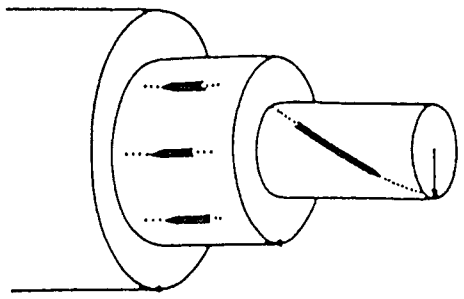

Figure 2. Theoretical model: two coaxial cylinders moving as solid bodies inside a motionless shell.

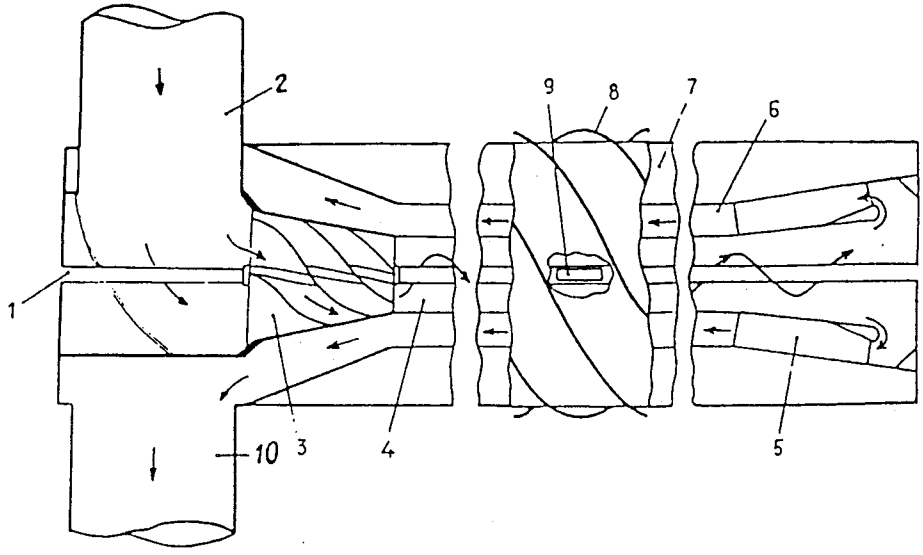

Figure 3. Experimental model. 1-Measuring channel. 2-Sodium entrance. 3-Helical labyrinth. 4-Main channel. 5-Reverse system. 6-Counterflow channel. 7-Immobile sodium. 8-Helical coil for outside excitation. 9-Coil, measuring transverse field. 10-Sodium exit.

$R_1 : R_2 : R_3 : L =$
$1 : 1.68 : 3 : 25$

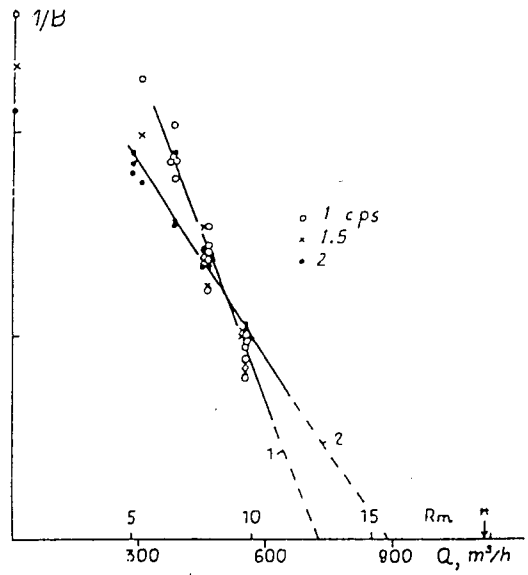

Figure 4. Measured $1/B$ signal versus flow rate Q for three frequencies.

Test of kinematic predictions

Gailitis et al. (2001)

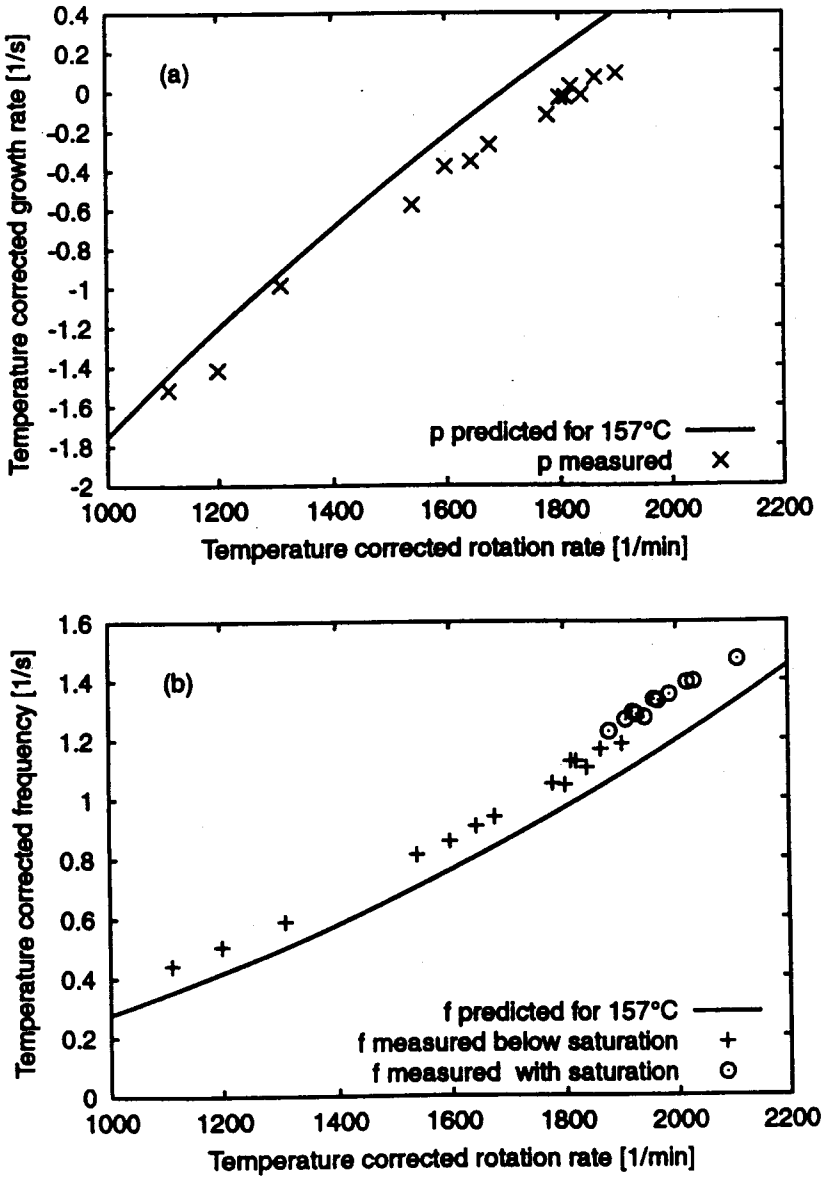

FIG. 4. Growth rates (a) and frequencies (b) for different rotation rates and temperatures in comparison with the numerical prediction. In (b) the frequencies in the saturation regime are also given, whereas the corresponding growth rates are zero.

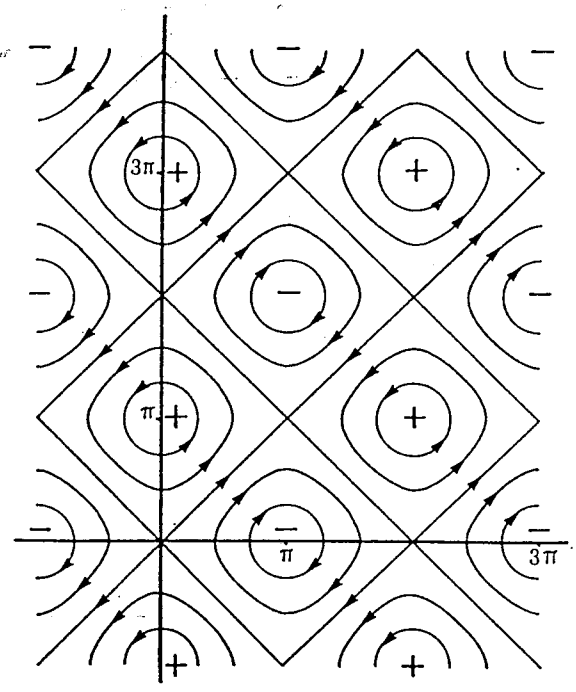

G.O. Roberts
(1972)

Karlsruhe
Dynamo

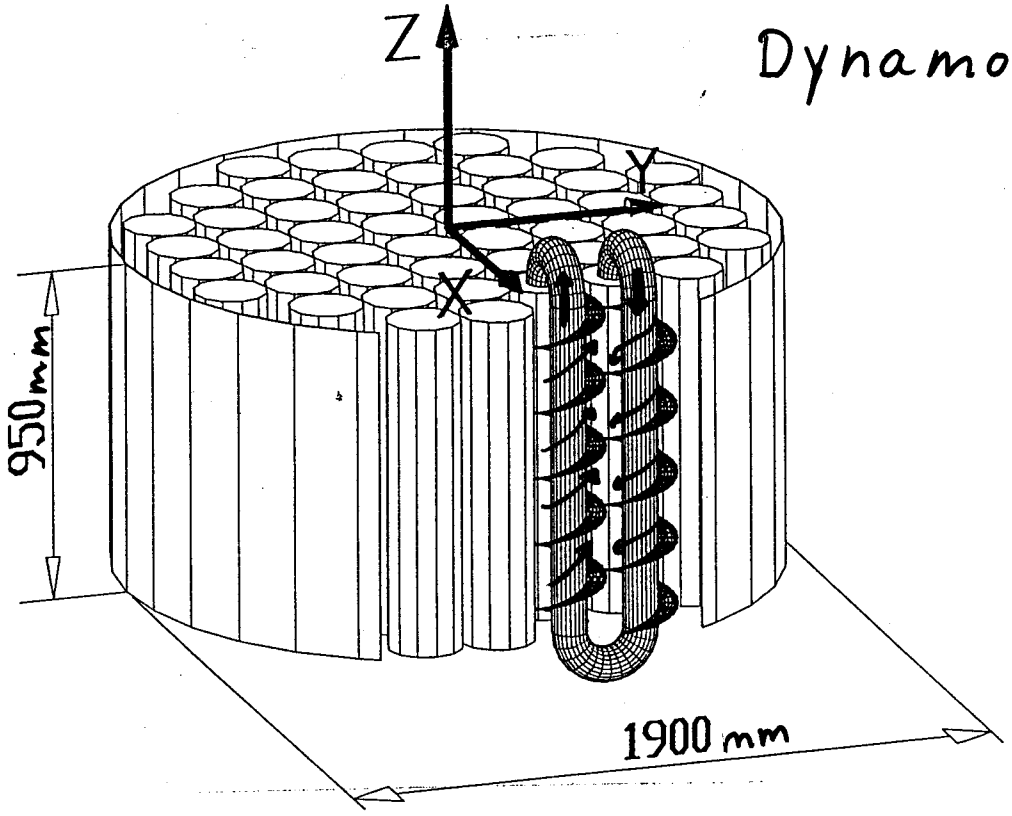

→ Multiple scale analysis

→ Numerical simulation

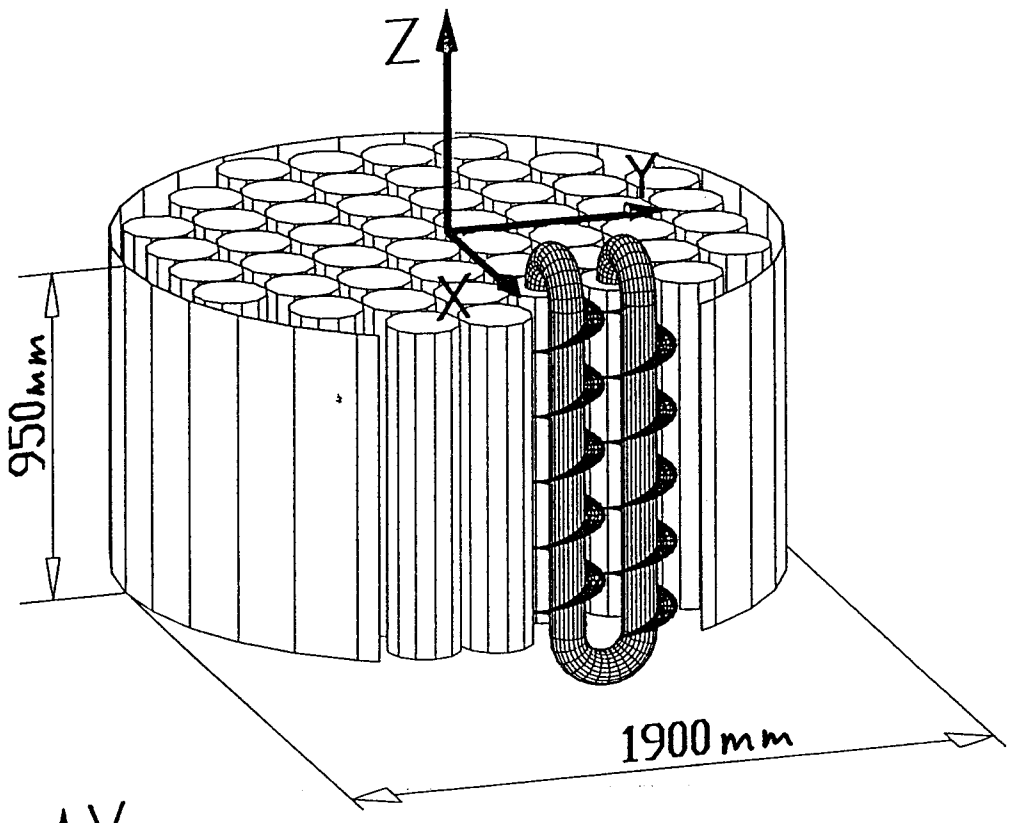
Z
Y
X
950mm
1900mm

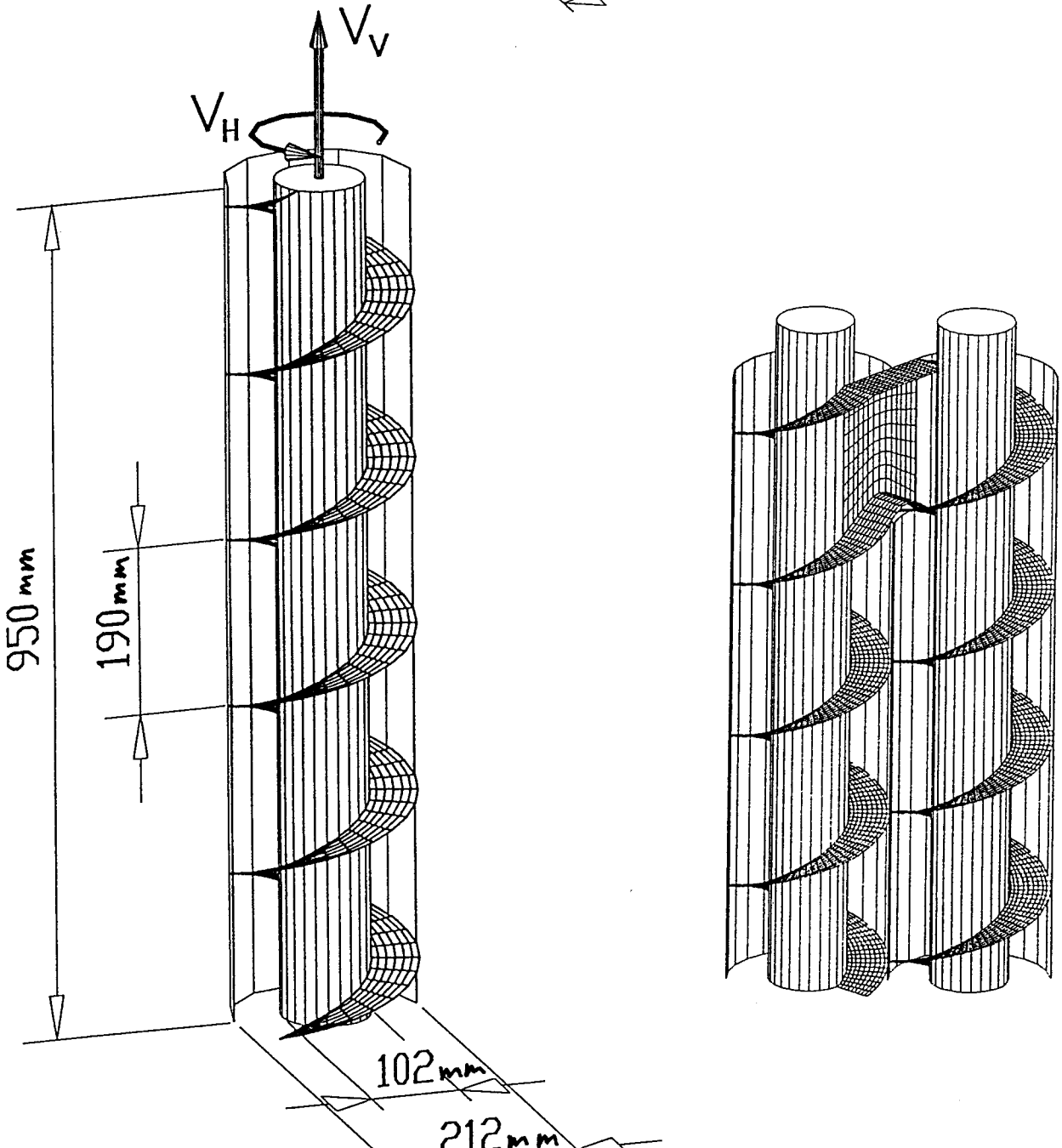
V_V
V_H
950mm
190mm
102mm
212mm

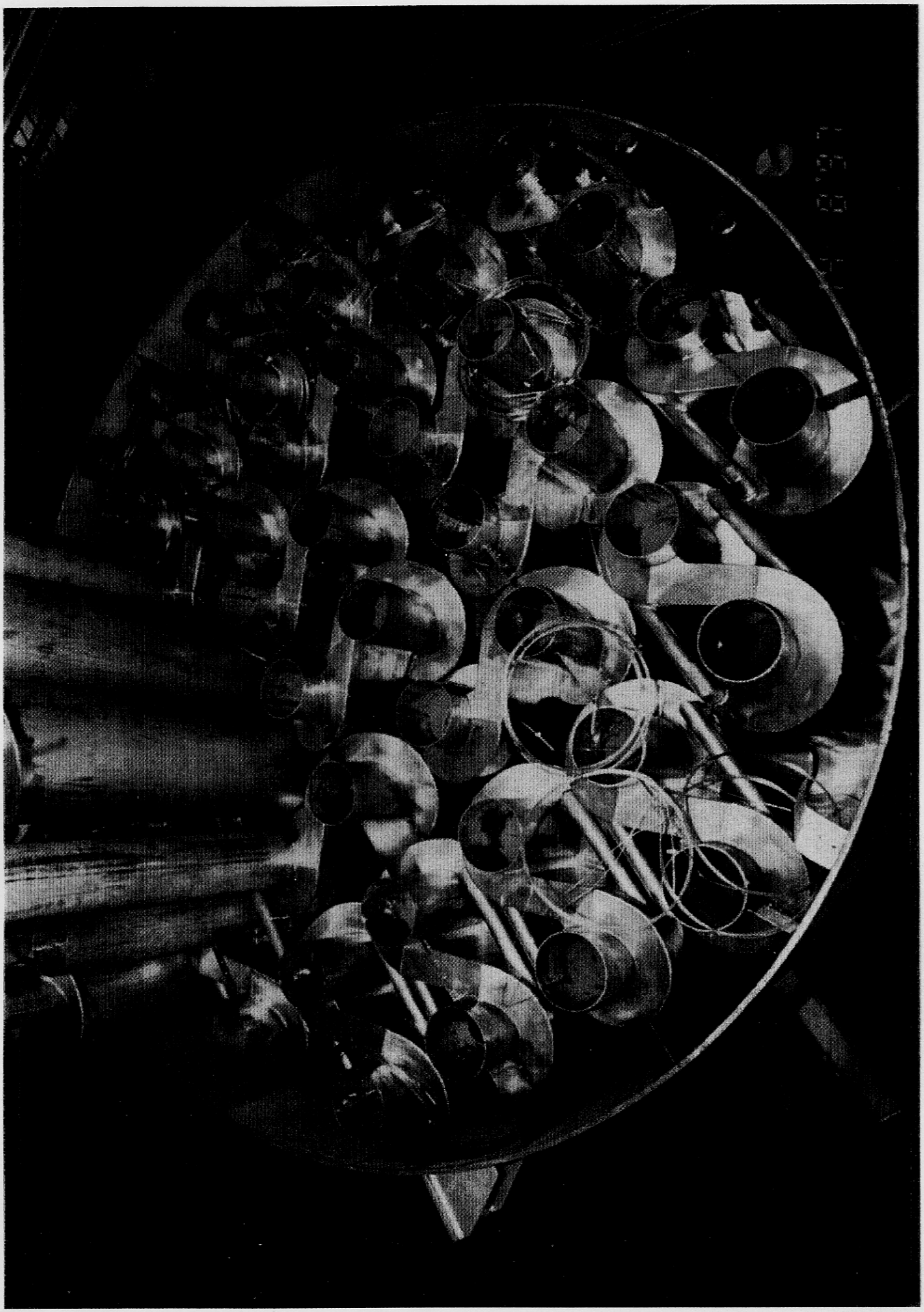

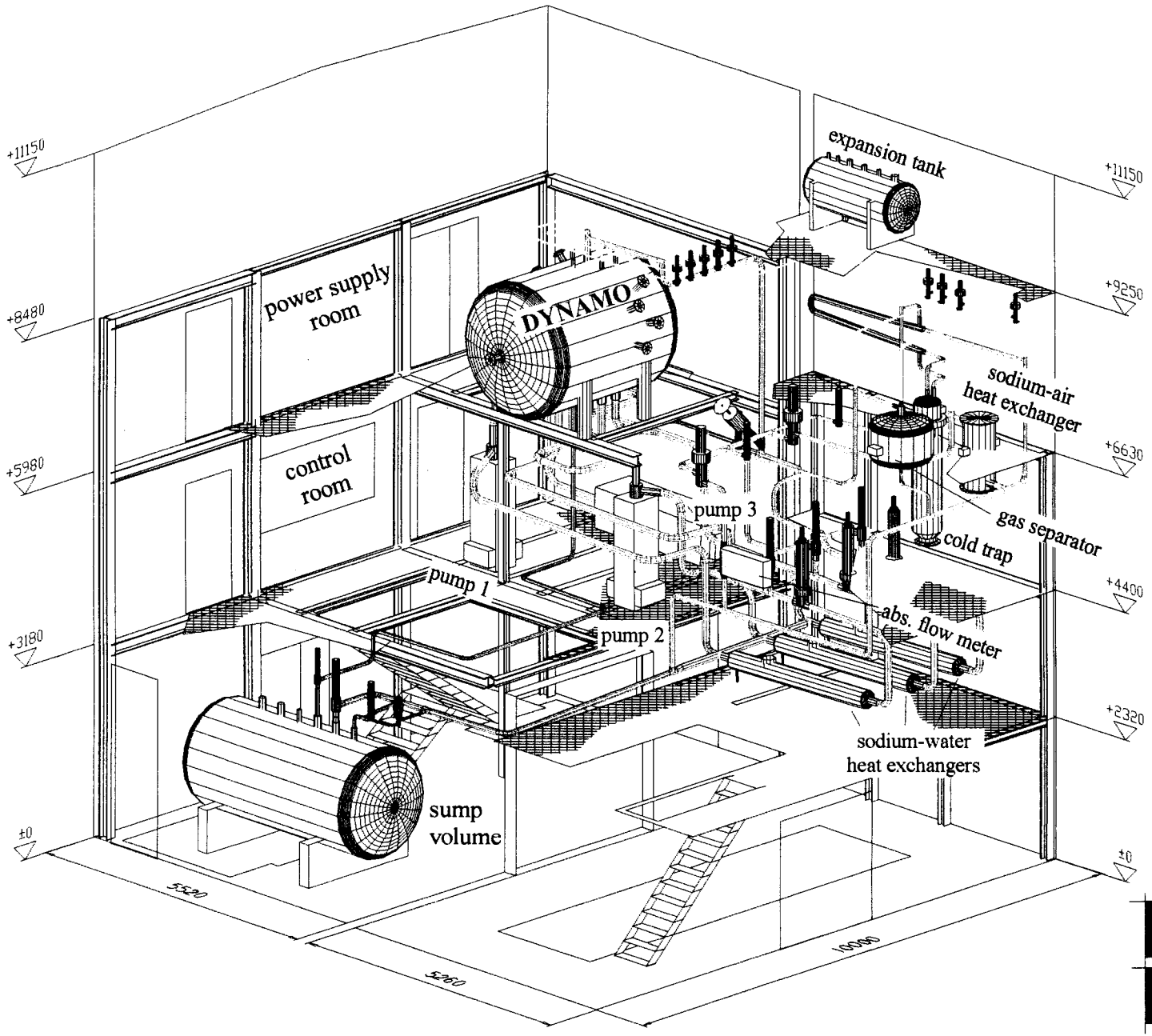

Forschungszentrum Karlsruhe
Technik und Umwelt

Institute for Applied Thermo- and Fluiddynamics (IATF)

The α-effect

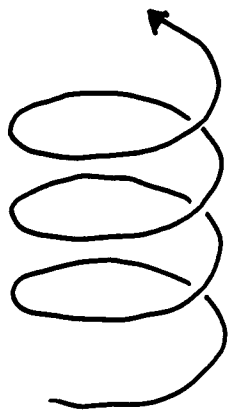

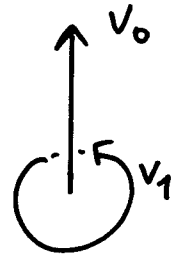

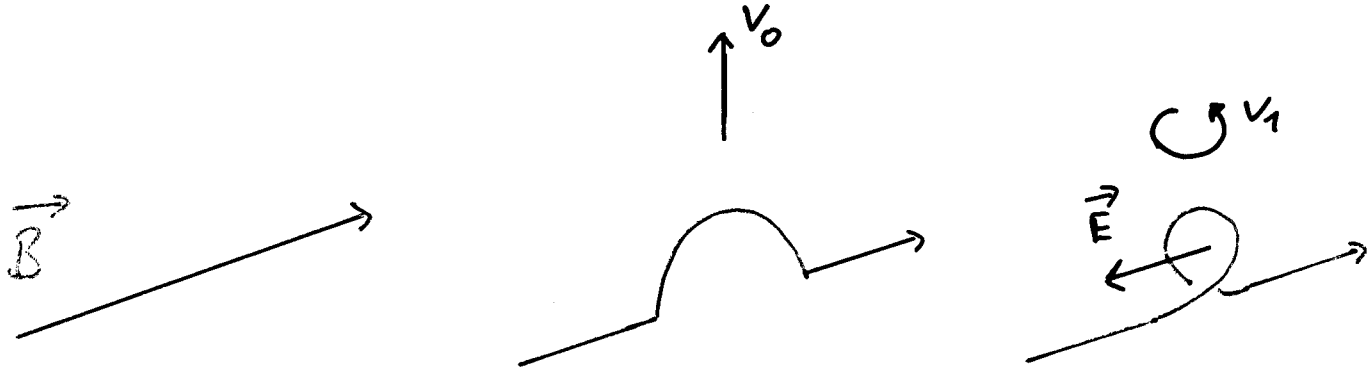

$$\vec{E} = \underline{\underline{\alpha}}\, \vec{B}$$

right handed helix $\rightarrow$ $\vec{E} \cdot \vec{B} \leq 0$

left " " $\rightarrow$ $\vec{E} \cdot \vec{B} \geq 0$

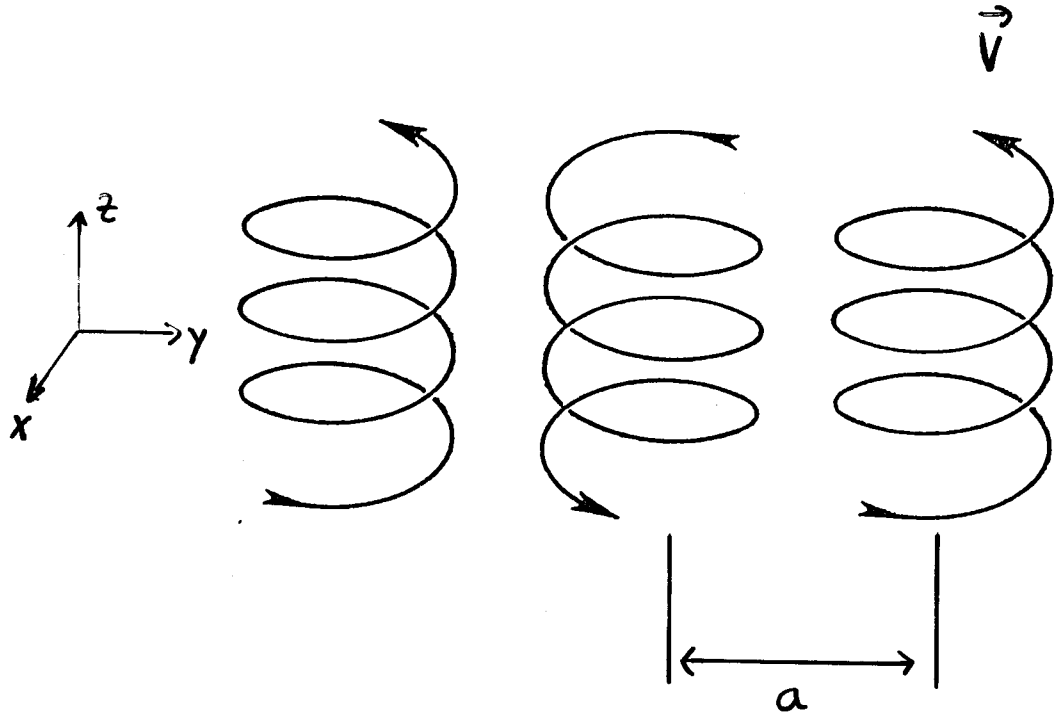

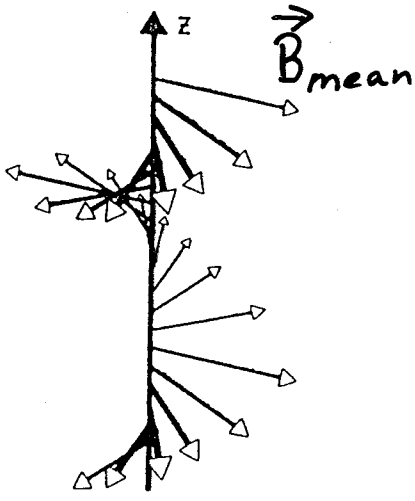

$$|\vec{B}_{mean}| \gg |\vec{B}_{fluct}|$$

for small $\frac{|\vec{v}| \cdot a}{\lambda}$

Direct Numerical Simulation of the Dynamo

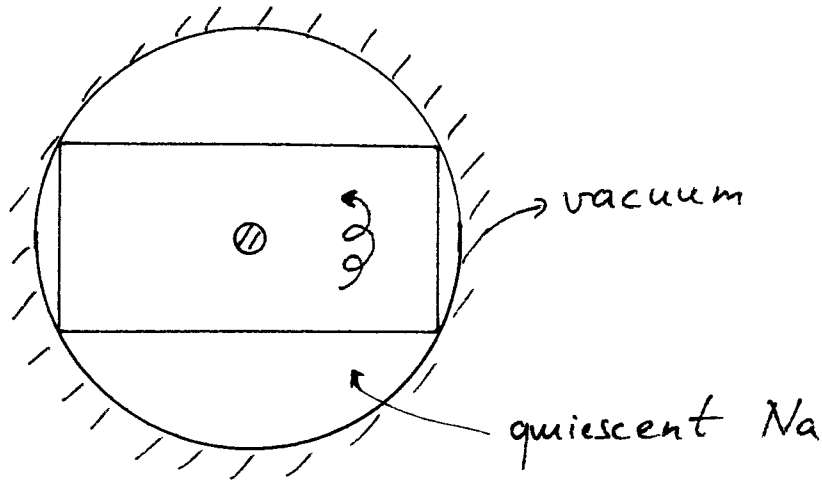

$$\frac{\partial \vec{B}}{\partial t} = \nabla \times (\vec{u} \times \vec{B}) + \frac{1}{R_m} \Delta \vec{B}$$

- spectral decomposition in Chebychev polynomials (radial) and Y_ℓ^m (angles)
- $u \times B$ computed in direct space
- time stepping with Adams-Bashforth / Crank-Nicholson
- CFL: $\Delta t < \left\{ \frac{r}{\sqrt{L(L+1)(u_\varphi^2 + u_\theta^2)}} \right\}_{min}$

$$\nabla^2 \longrightarrow \frac{\partial^2}{\partial r^2} - \frac{\ell(\ell+1)}{r^2}$$

↳ exclude origin

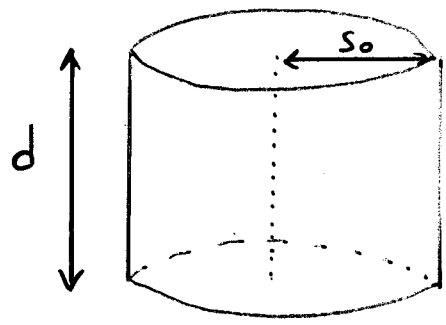

$S_o/d = 1$

$S_o/d = 1.2$

$\lambda = 0.11$ $0.115\ \frac{m^2}{s}$

$\lambda = 0.1\ \frac{m^2}{s}$

experiment

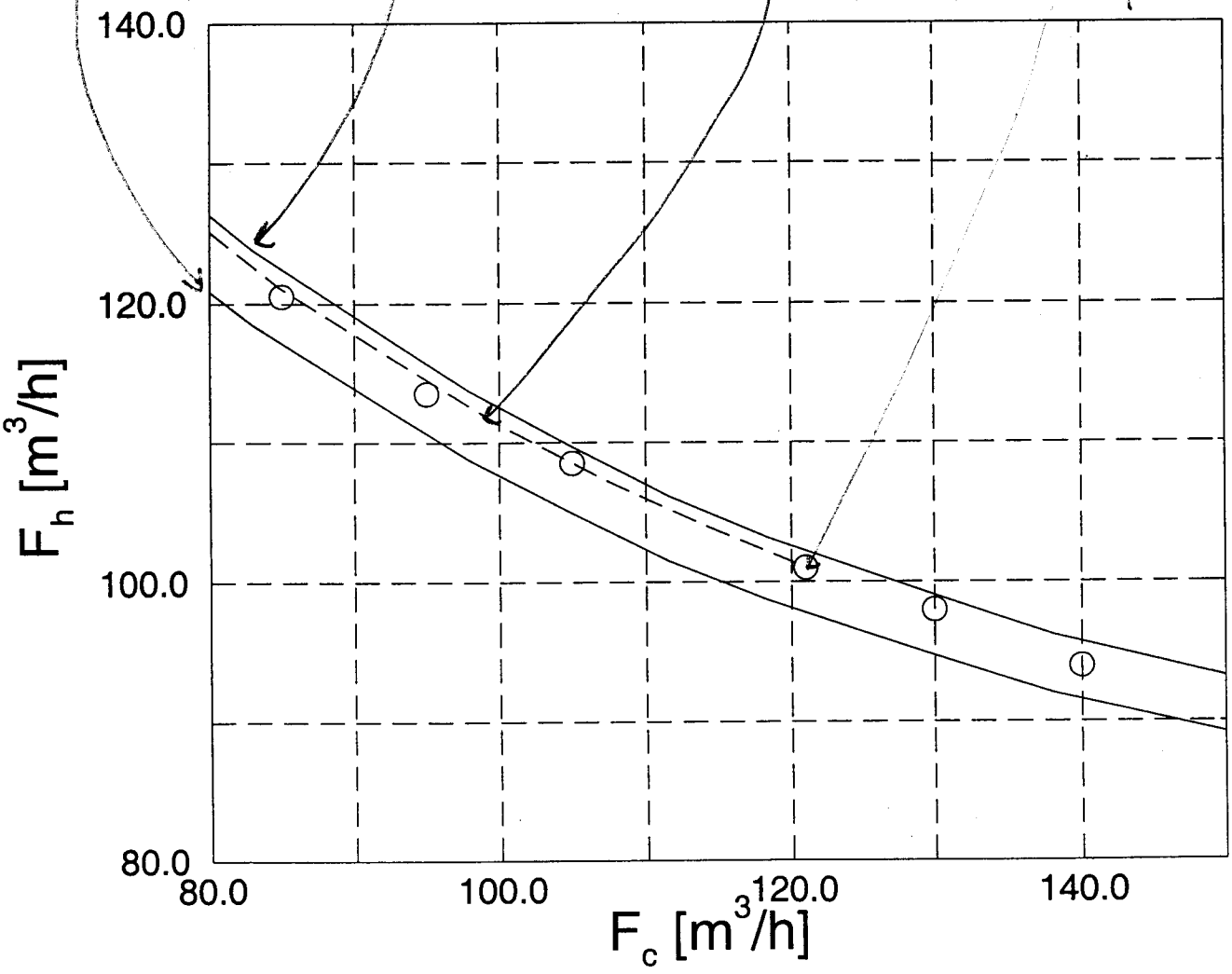

B_r

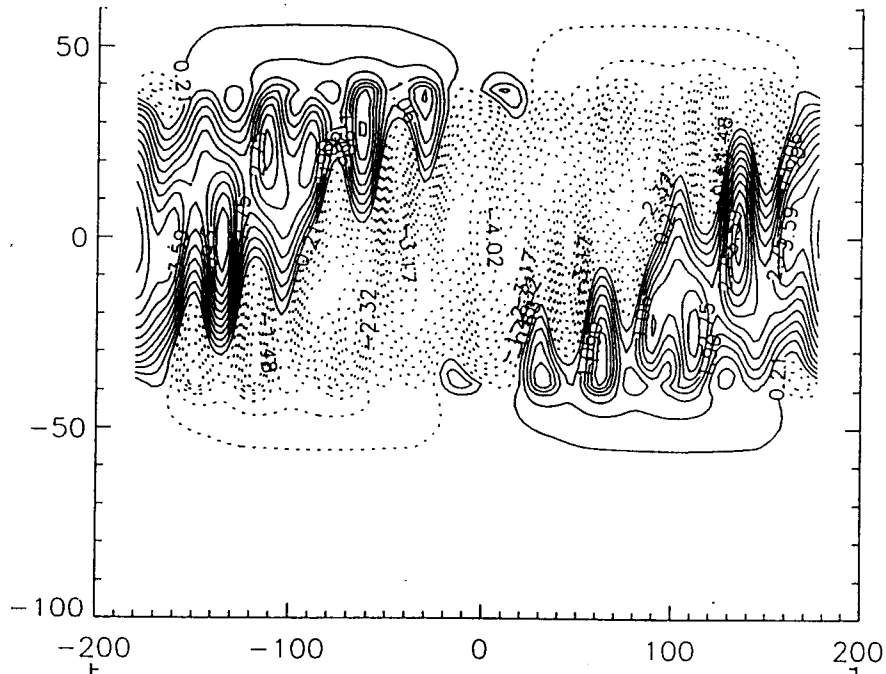

cylindrical surface

$s = 0,638$

B_z

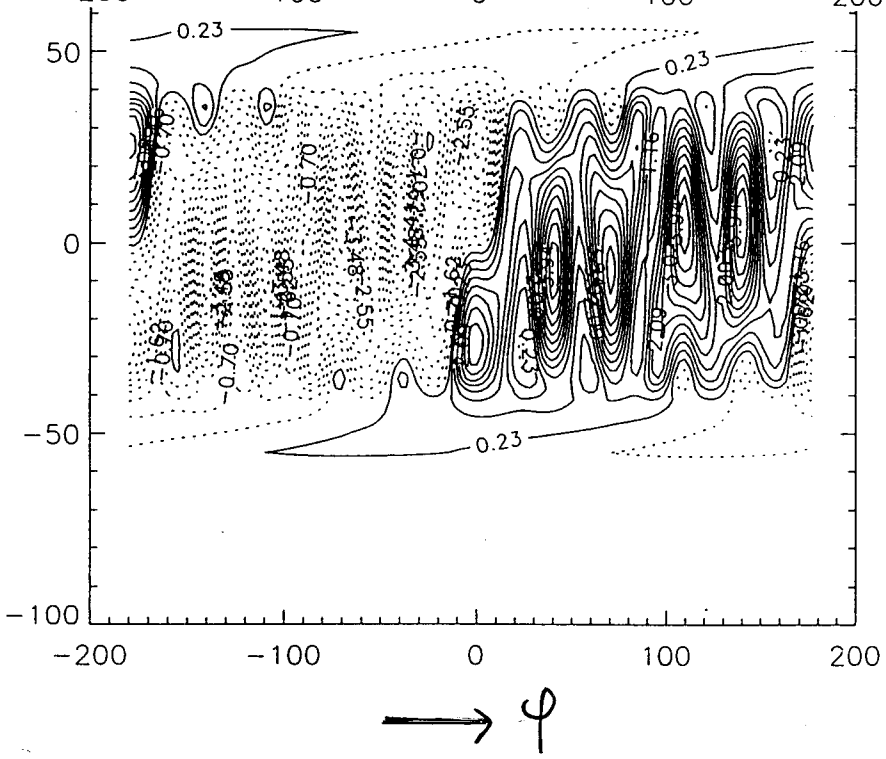

$\longrightarrow \varphi$

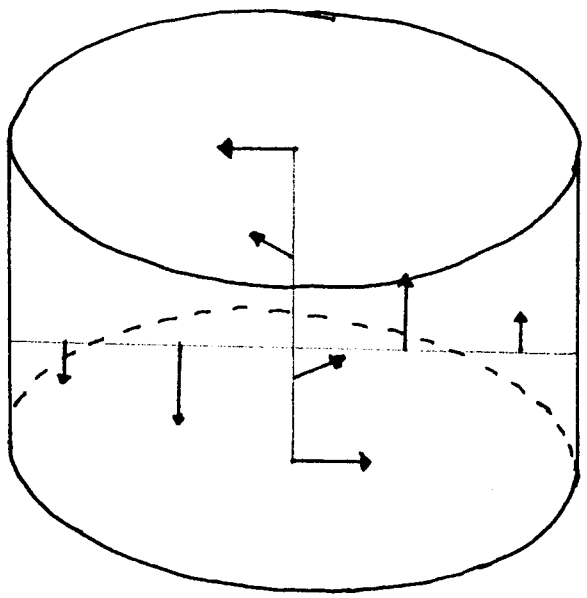

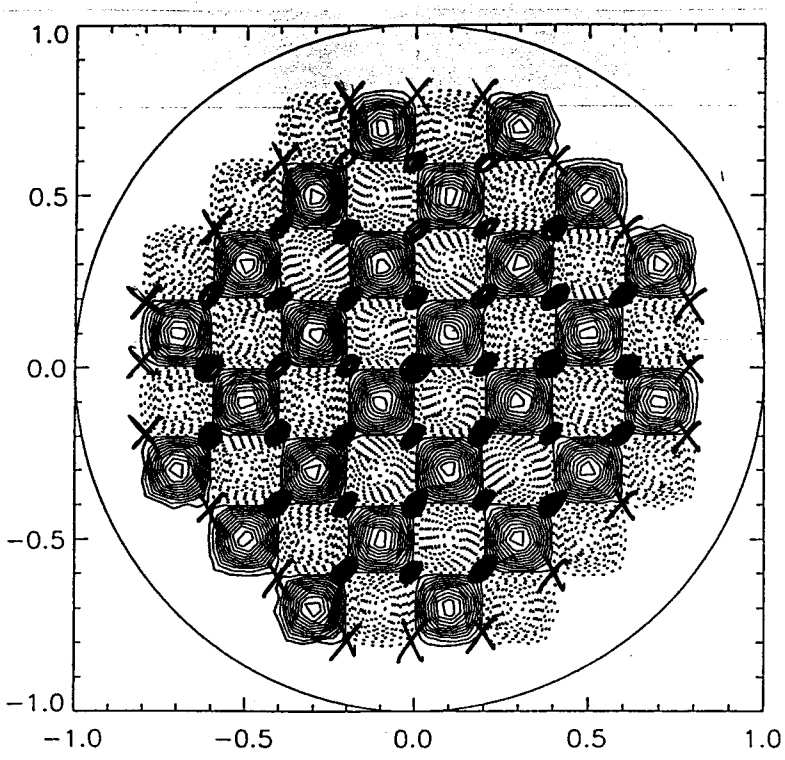

● 21

● 16

X 4

X 16

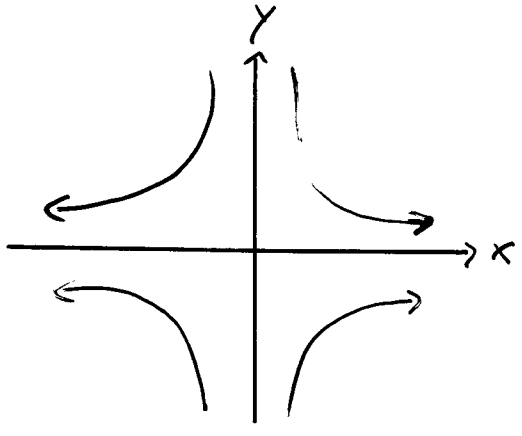

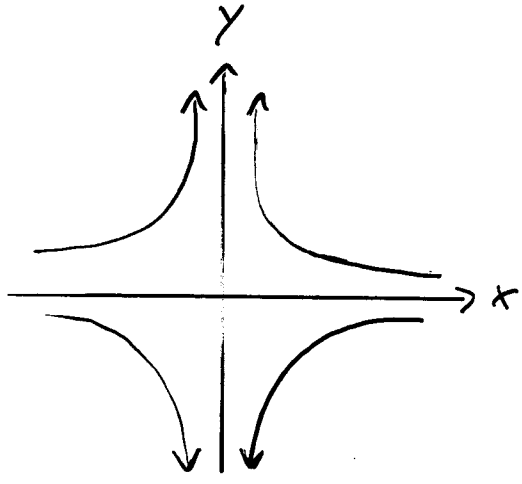

B-field at the origin

along x : $Rm_{crit} = 14.77$

along y : $Rm_{crit} = 14.99$

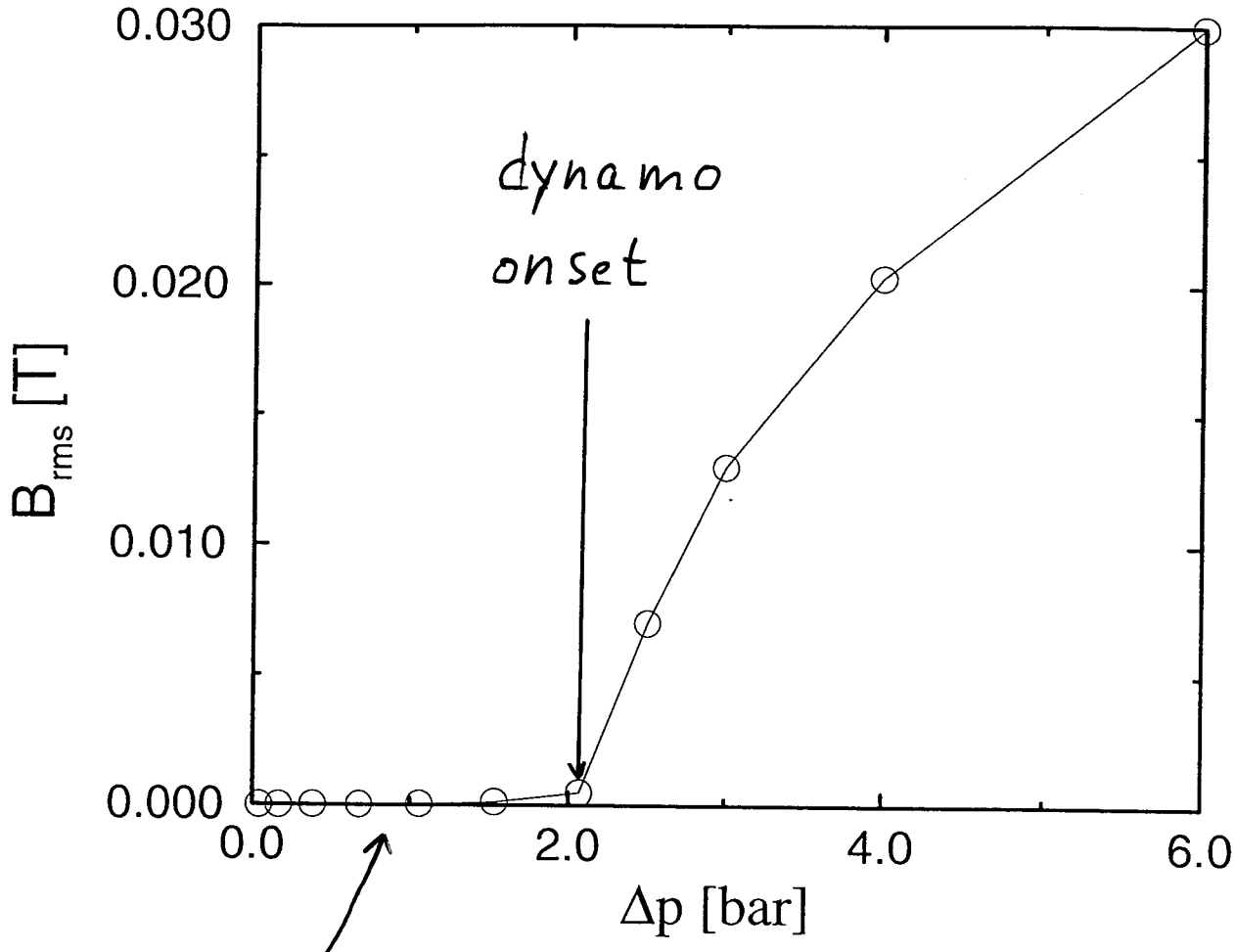

amplification of ambient magnetic field

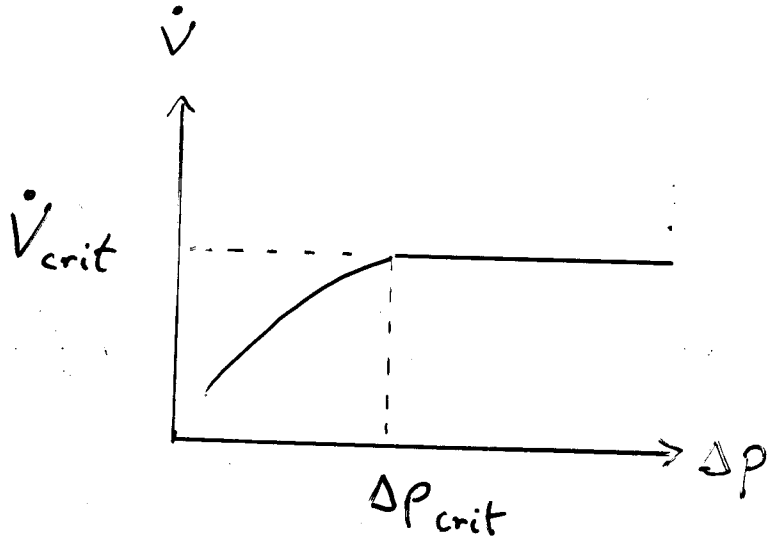

boundary conditions : $\eta=(ms)^{-1}=0.1m^2/s$, $V_{central}=101m^3/h$, T=125°C

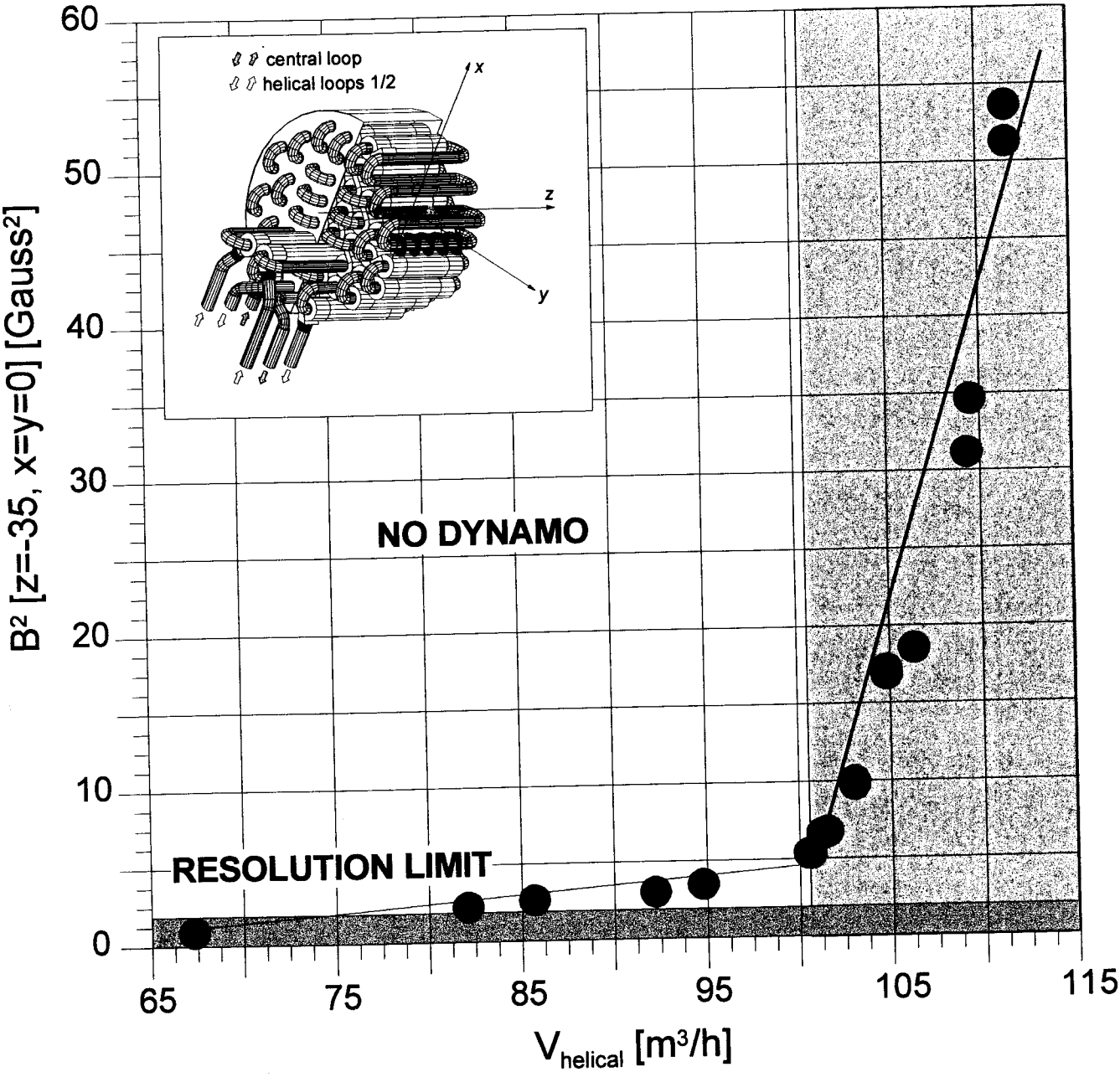

Saturation

$$\frac{\partial}{\partial t}\vec{v} + (\vec{v}\nabla)\vec{v} = -\nabla p + \frac{1}{Re}\nabla^2\vec{v} + \vec{f} + (\nabla\times\vec{B})\times\vec{B}$$

$$\frac{\partial}{\partial t}\vec{B} + \nabla\times(\vec{B}\times\vec{v}) = \frac{1}{Rm}\nabla^2\vec{B}$$

$$\nabla\cdot\vec{v} = \nabla\cdot\vec{B} = 0$$

Laminar flow near onset of dynamo:

perturbation expansion

Ponomarenko: Nunez et al. (2001)

G.O. Roberts: Tilgner & Busse (2001)

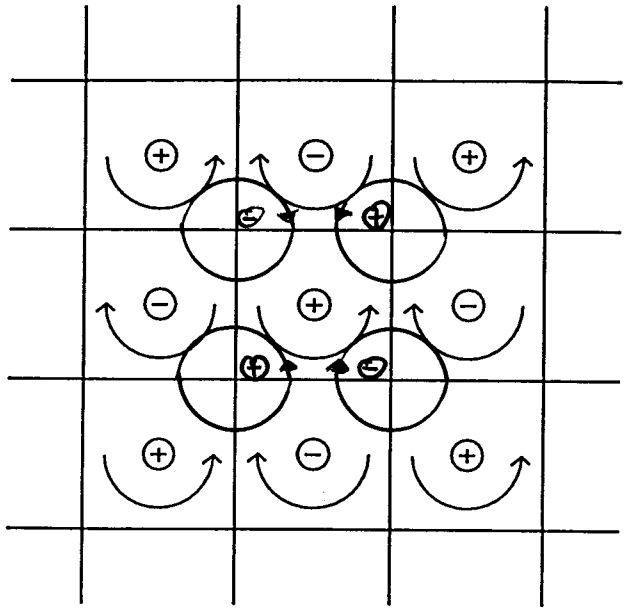

$Z > 0$

$$\vec{V}_{tot} = (1-\gamma)\,\vec{V}_0 + \gamma\,\vec{V}_1 \qquad \gamma \propto |\vec{B}|^2$$

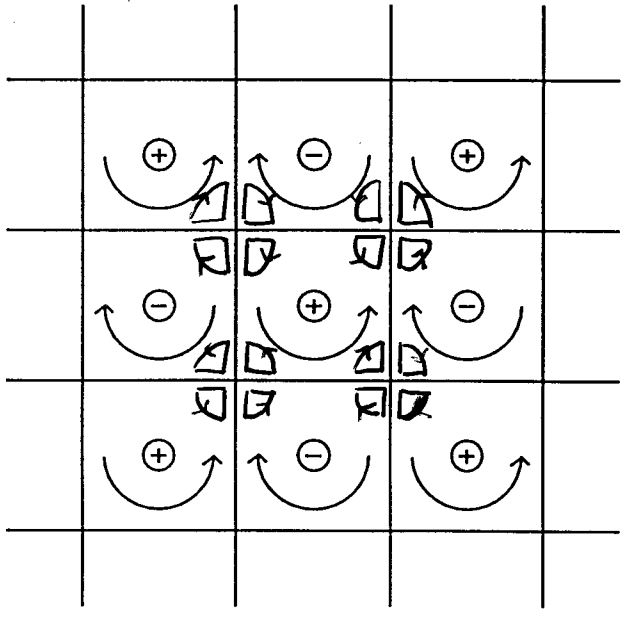

$Z > 0$

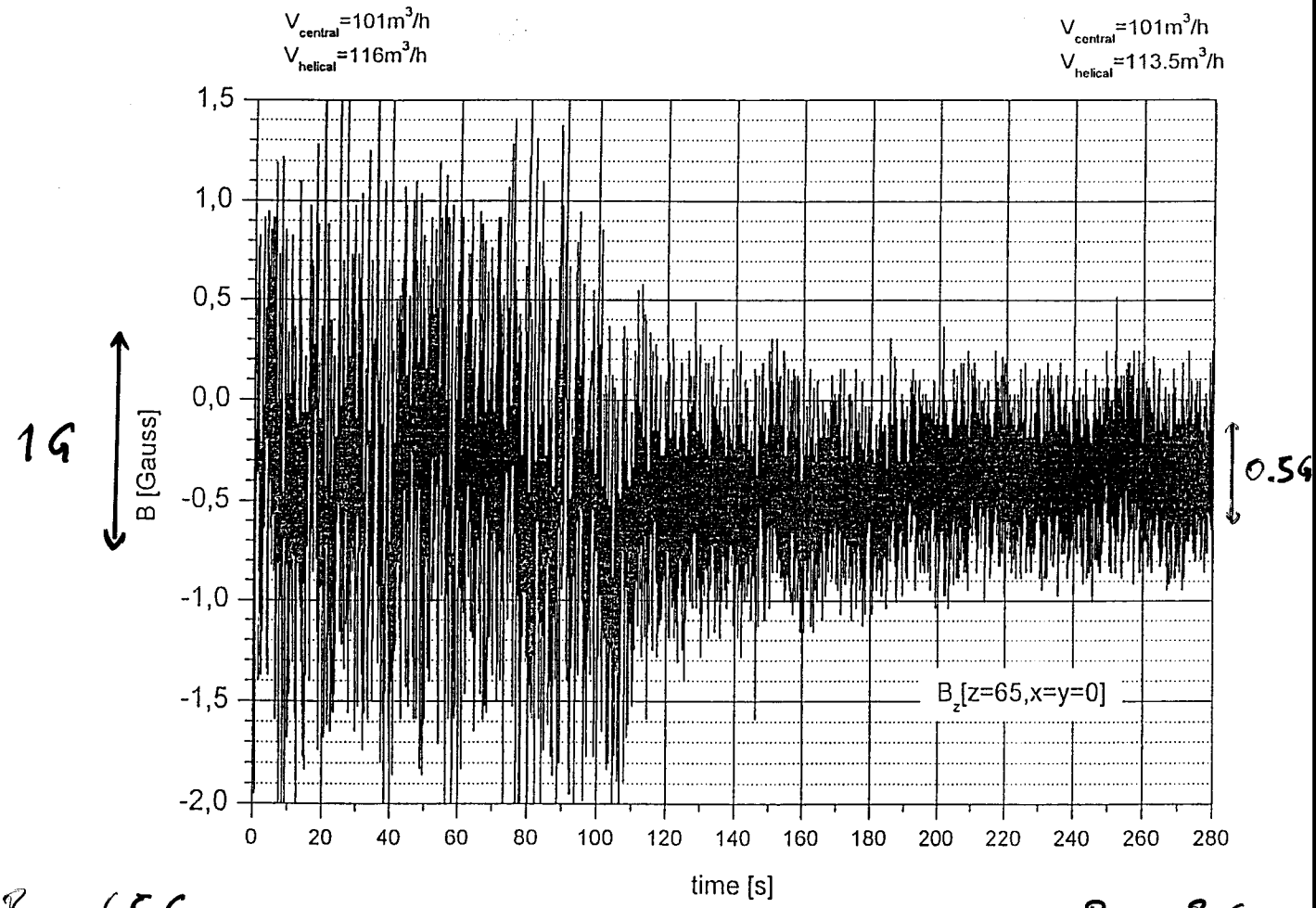

$B_x = 6.5\,G$

$B_y = -2.7\,G$

$B_x = 8\,G$

$B_y = -9\,G$

$$\lambda \nabla^2 \vec{b} \approx \vec{B} \nabla \vec{u}$$

$\vec{b}, \vec{u}$ fluctuating components

$$\Rightarrow \left|\frac{b}{B}\right| \approx \frac{1}{\lambda}\frac{a}{\pi}|u|$$

$$= 0.64\,\frac{s}{m}\,|u|$$

$|u| \approx 0.022\,\frac{m}{s} \longrightarrow |u| \approx 0.065\,\frac{m}{s}$

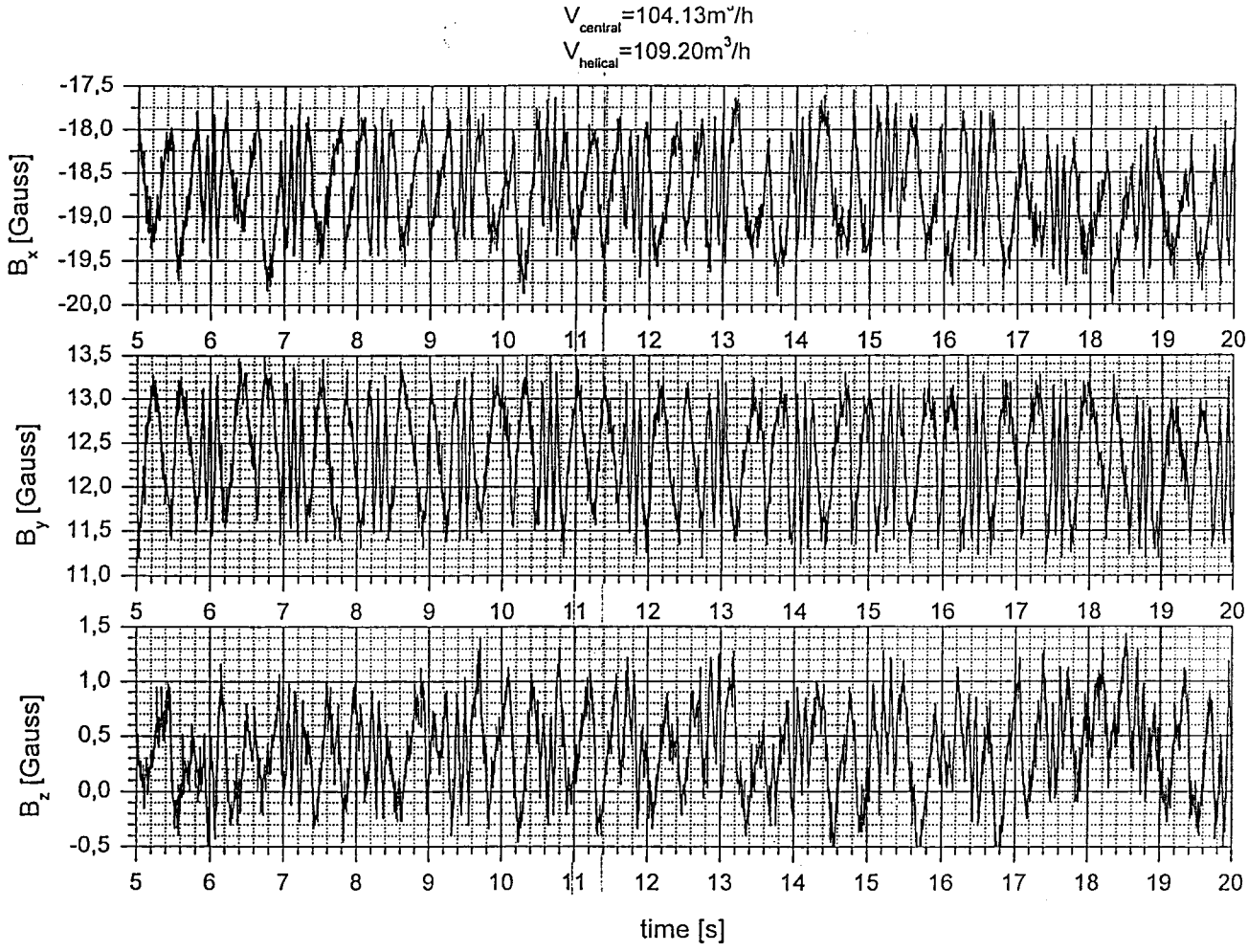
$V_{central}$=104.13m^3/h
$V_{helical}$=109.20m^3/h
B_x [Gauss]
B_y [Gauss]
B_z [Gauss]
time [s]

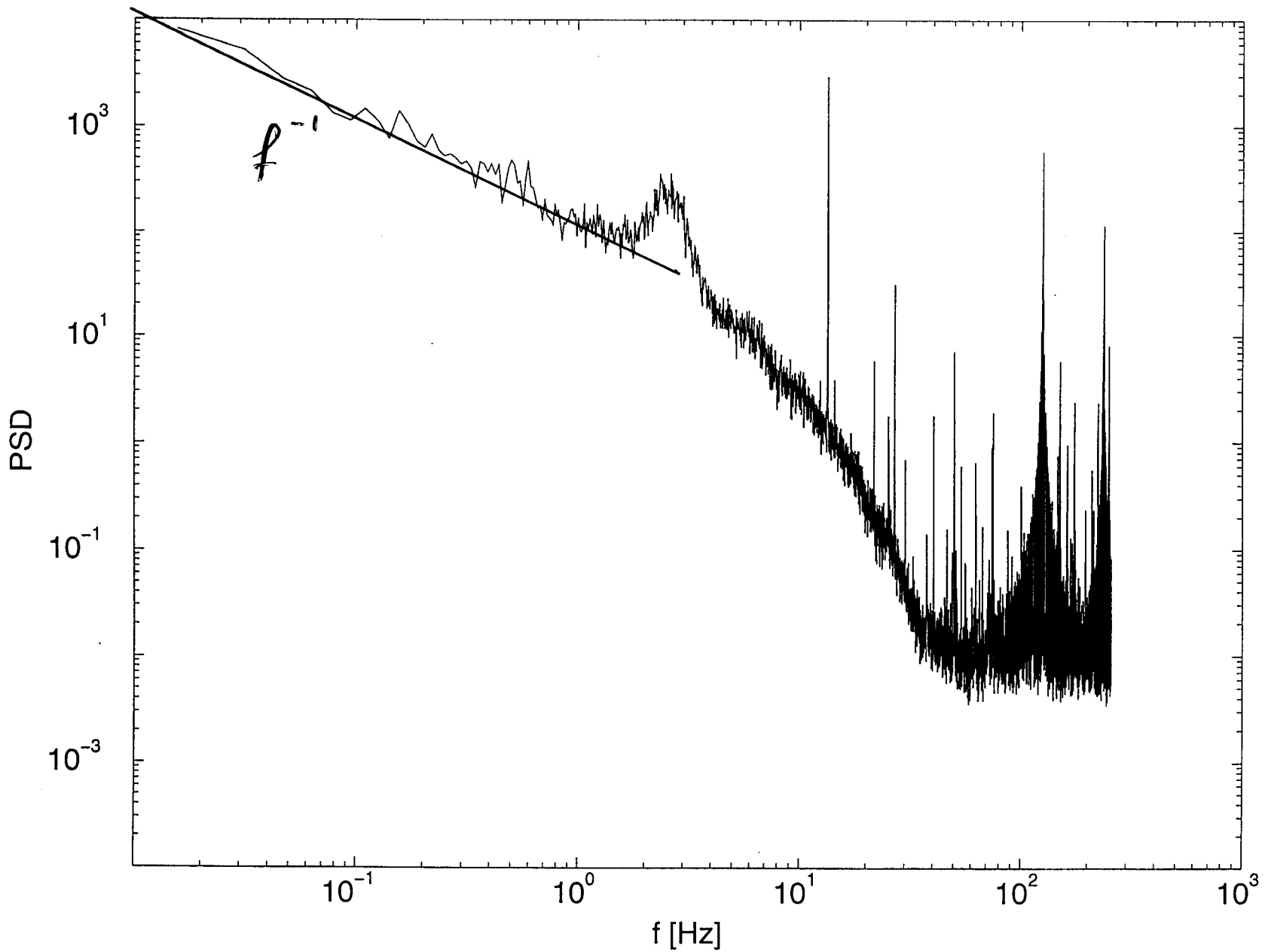
f^{-1}
10^3
10^1
10^{-1}
10^{-3}
PSD
10^{-1}
10^0
10^1
10^2
10^3
f [Hz]

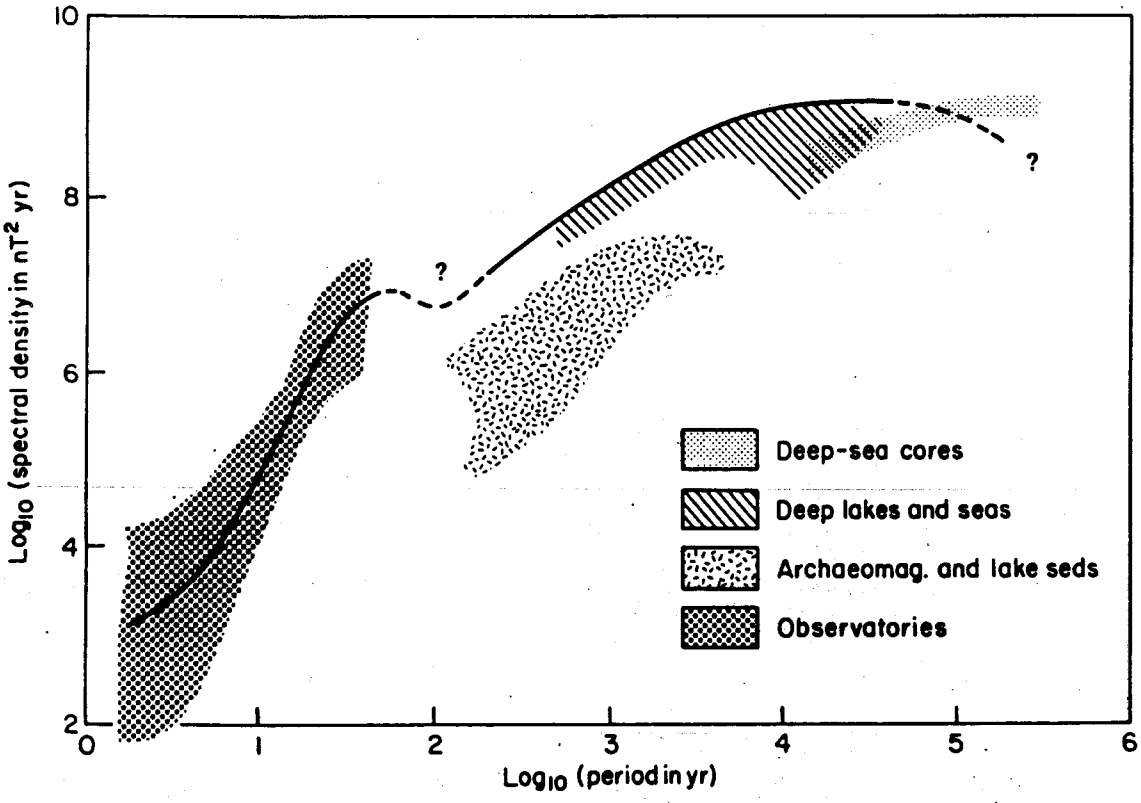

Fig. 4.18. Continuous geomagnetic power spectrum derived from observatory and palaeomagnetic data. (After Barton, 1983.)

- Dynamo action starts at $\dot{V} \approx 100\ m^3/h$
- sign of $\vec{B}$ depends on initial conditions
- saturation field up to 200 G
- orientation of $\vec{B}$

- dynamic effects:
  - $\dot{V}$ increases beyond its critical value
  - turbulence reduced by B
  - regular oscillations (at high B ?)
  - change of orientation of $\vec{B}$!

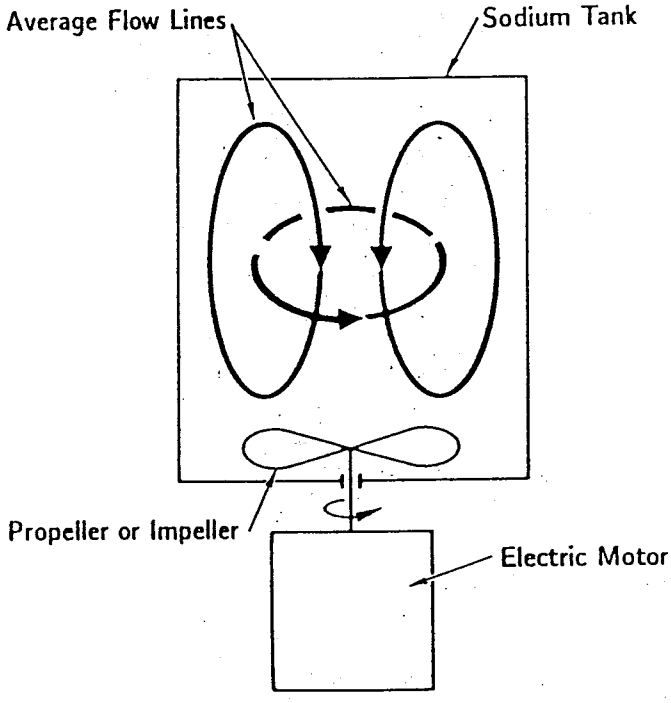

P.H. Roberts & Jensen (1993)

"projet Ampère" France

D. Lathrop Maryland

C. Forest Madison

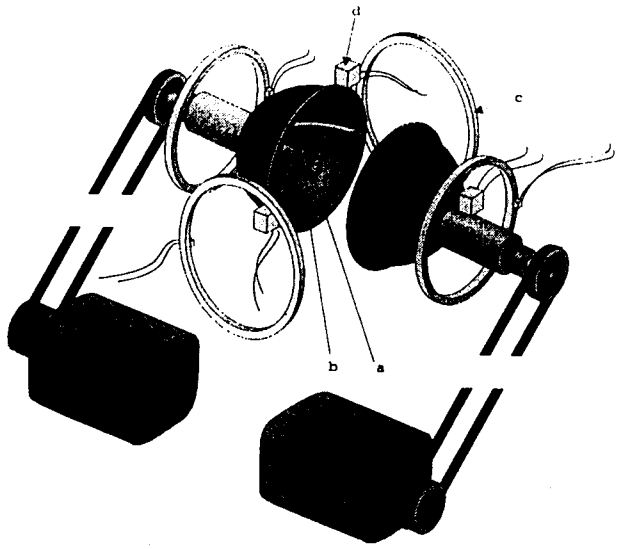

Figure 1. An exploded view of the experiment shows the propellers (a) and poloidal baffles (b) inside the sphere. The Helmholtz coils (c) and hall probes (d) are located outside the sphere.

Peffley, Cawthorne, Lathrop (2000)

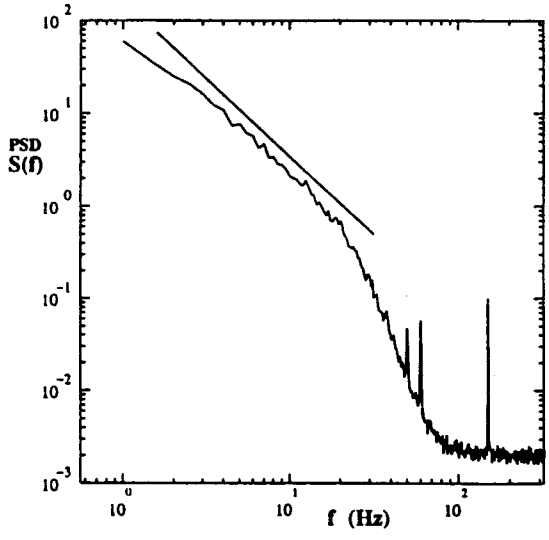

FIG. 12. The power spectral density of induced field fluctuations shows broadband turbulent features including a power law decay at low frequency. An offset line is shown with the best fit exponent $S(f) \sim f^{-1.68\pm0.03}$. This is consistent with the scaling indicated by Eq. 8. Also prominent are peaks at $\Omega/2\pi = 50Hz$, power line interference at $f = 60Hz$ and one at $3\Omega/2\pi = 150Hz$. The magnetic Reynolds number for this flow is 33.

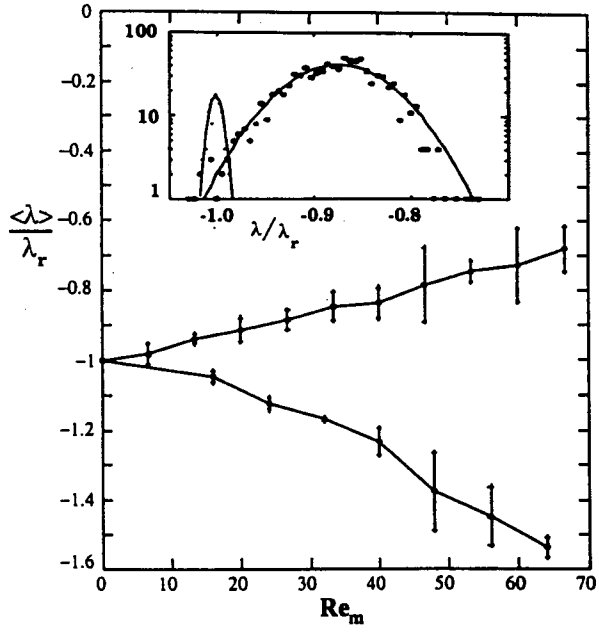

FIG. 6. The mean eigenvalue dependence on magnetic Reynolds number shows a shift toward self-generation for fields aligned with the shafts (solid line) and a shift away from self-generation for fields at right angles to the shafts (dashed line). The error bars indicate shot-to-shot fluctuations in the eigenvalue estimates. These fluctuations are further quantified by the distribution of eigenvalues shown in the inset for 895 observations of the eigenvalue while at the same $Re_m = 42$. All the eigenvalues in this figure are normalized to yield -1 in conditions of no flow. The distribution for no flow ($Re_m = 0$) is shown in the inset by the narrow Gaussian around -1. Presumably, the self-generating state is achieved if we cross the $\lambda = 0$ line.

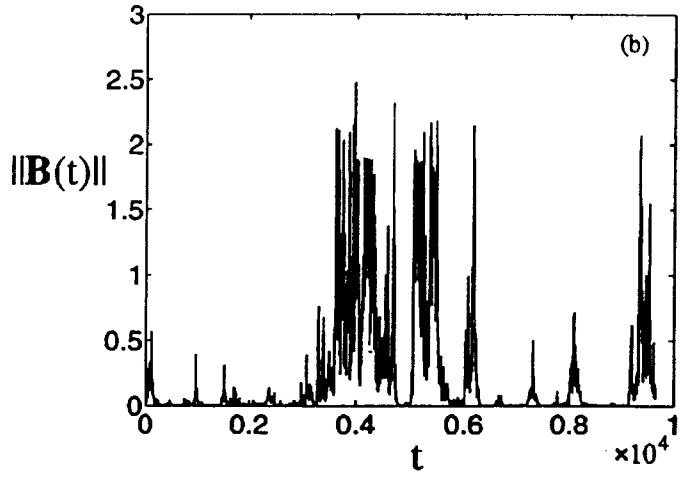

blowout bifurcation ?

Sweet et al. 2001

FIG. 1. (a) $||\mathbf{B}||$ versus t from our MHD computations at $(R_m - R_{mc})/R_{mc} = 0.010$. (b) $||\mathbf{B}||$ versus t for $(R_m - R_{mc})/R_{mc} = -0.015$ and an applied field of 1.6×10^{-4} in the x direction.

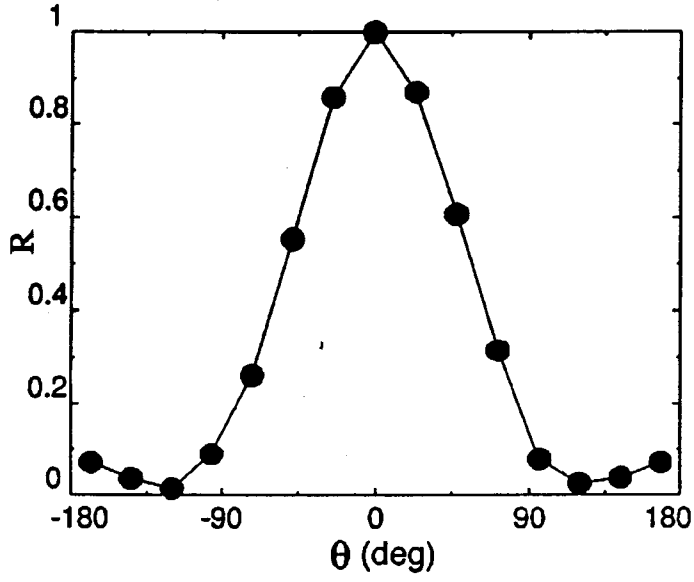

Peffley et al. 2000

FIG. 9. The coefficient of regression ($R = 1$ gives perfect linear dependence) from linear regressions of instantaneous eigenvalues from Hall probes separated by an azimuthal angle Θ. These data are taken at $\mathrm{Re}_m = 42$.

Tilgner 2002 : Interpretation in terms of transients

$$\frac{\partial}{\partial t}\vec{B} + R_m \nabla \times (\vec{B} \times \vec{v}) = \nabla^2 \vec{B}$$

$$\vec{v} = \varepsilon \nabla \times \nabla \times f_p(r) P_2(\cos\vartheta)\hat{r} + \nabla \times f_t(r) P_2(\cos\vartheta)\hat{r}$$

$$f_t(r) = r(1-r)\sin(\pi r), \quad f_p = r f_t(r)$$

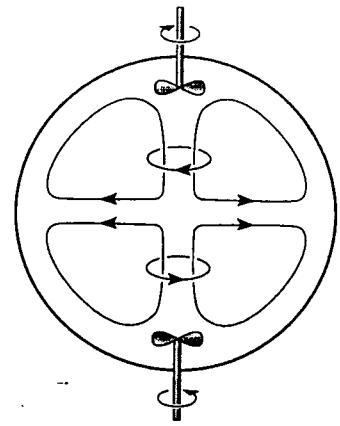

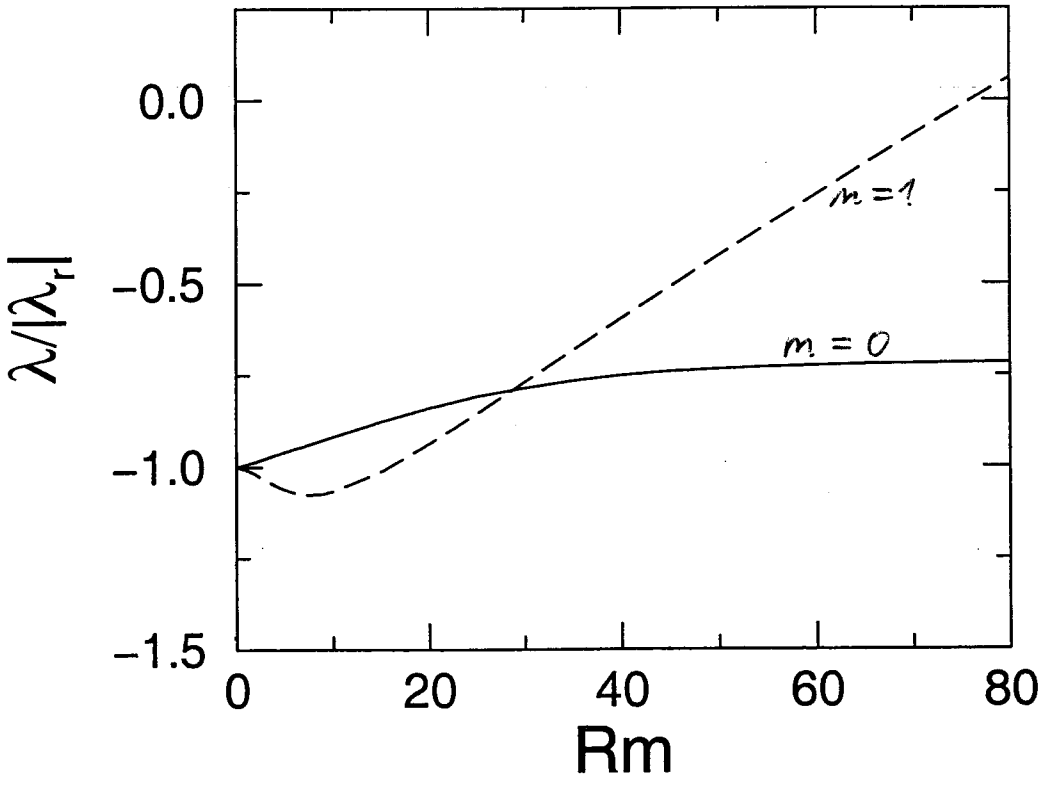

$\varepsilon = 0.25$

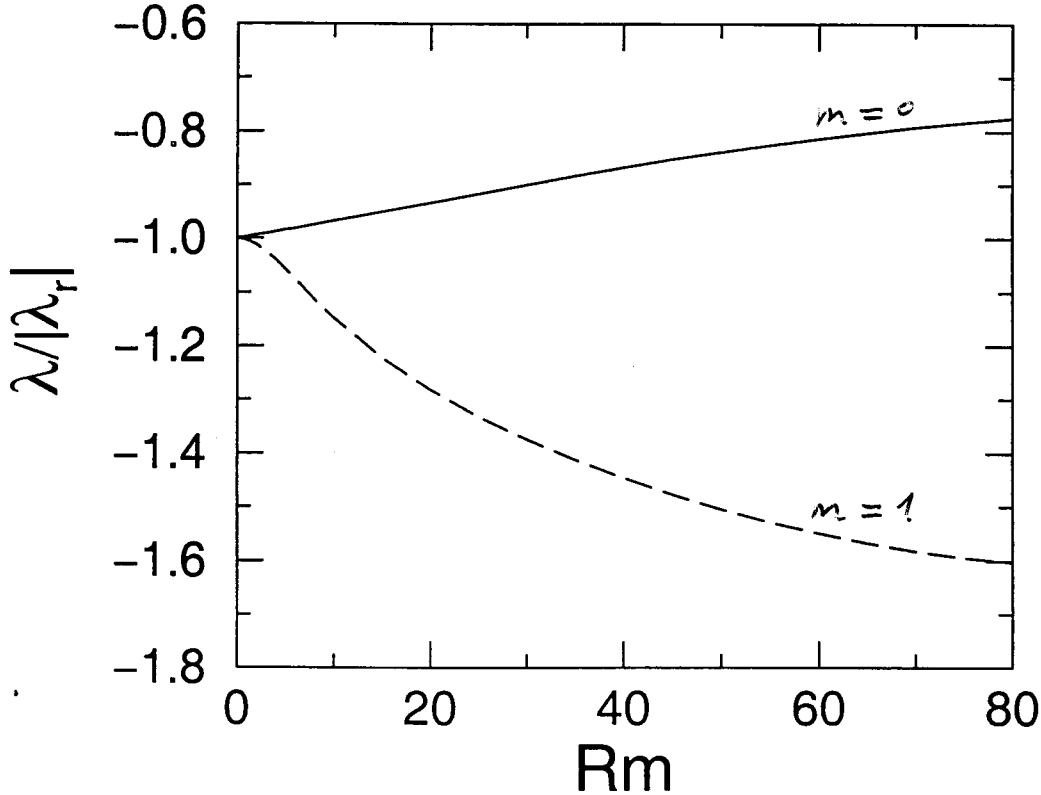

$\varepsilon = 0.1$

Eddy diffusivity

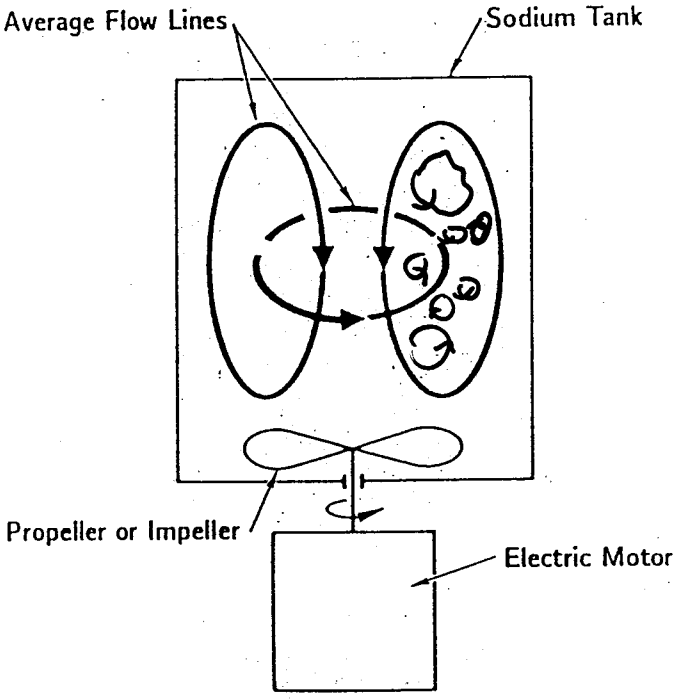

$L = 1\,m$

$Rm = 100 \rightarrow V = 10\ \frac{m}{s}$

$\rightarrow V_{rms} \overset{?}{\doteq} 1\ \frac{m}{s}$

$l_{eddy} \overset{?}{\doteq} 0.1\,m$

$\Rightarrow \lambda_{eddy} = 1\ \frac{m}{s} \cdot 0.1\,m = 0.1\ \frac{m^2}{s}$

$= \lambda_{molecular}$!

C. Forest (1998)

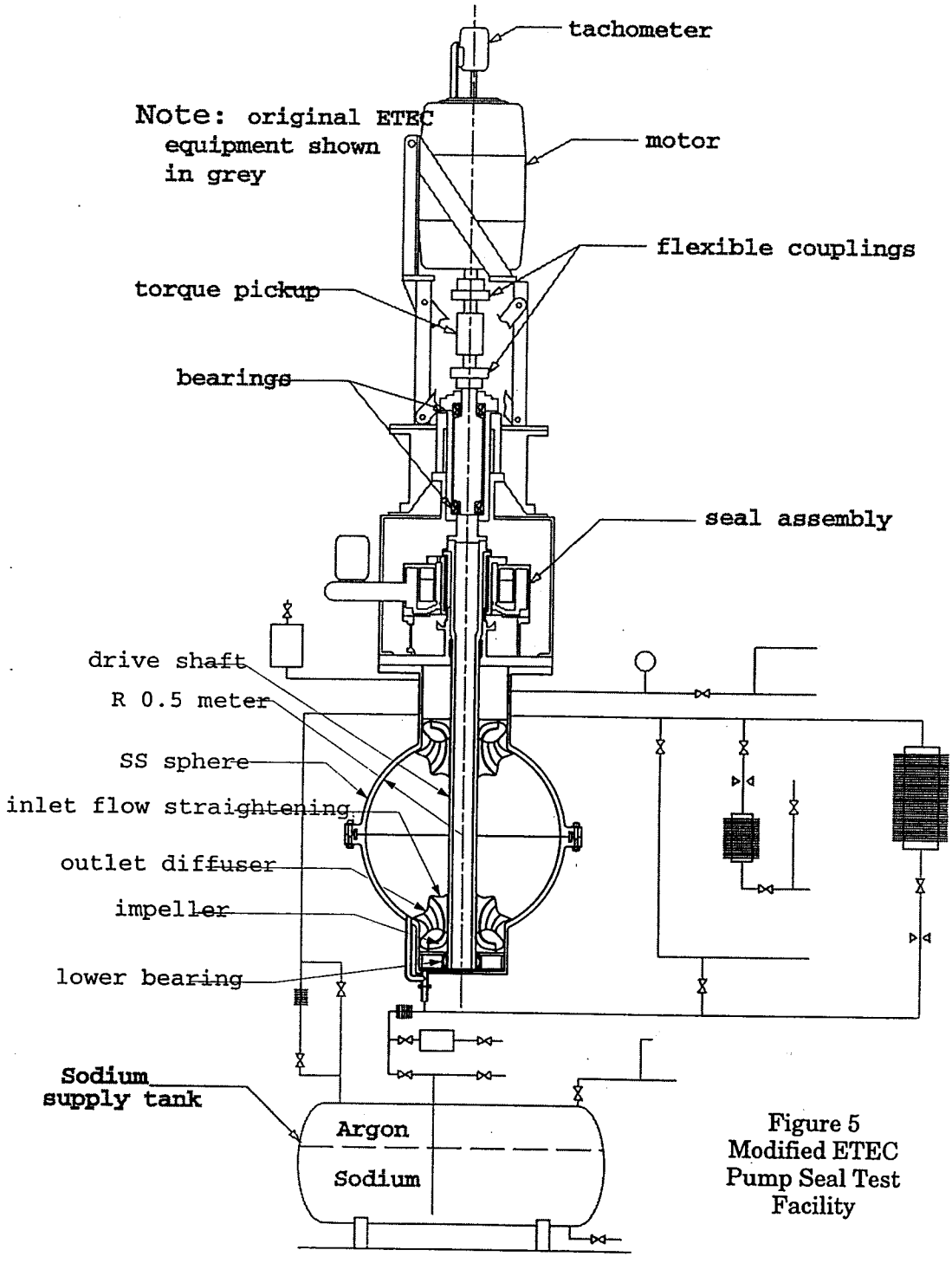

Figure 5: Schematic of the modified Pump Seal Test Facility from ETEC. The hardware shown in gray is an existing test stand which can be brought the the University of Wisconsin. The spherical vessel shown in black is the primary modification to the facility which would be required for the dynamo experiments. The holding capacity of the sodium supply tank is 140 gallons, which will accomodate a 50 cm radius sphere. The ETEC equipment includes the rotary feedthrough, bearings, heaters, superstructure, and 50 Hp motor necessary to handle the experiment. The vessel will be constructed out of nonmagnetic stainless steel. The impellers are shown with straightening fins for constroling the ratio of toroidal to poloidal velocity. The ancilliary loops are used to purify the sodium.

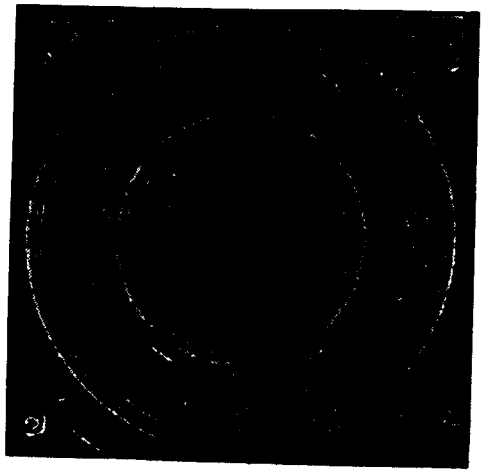

Perm

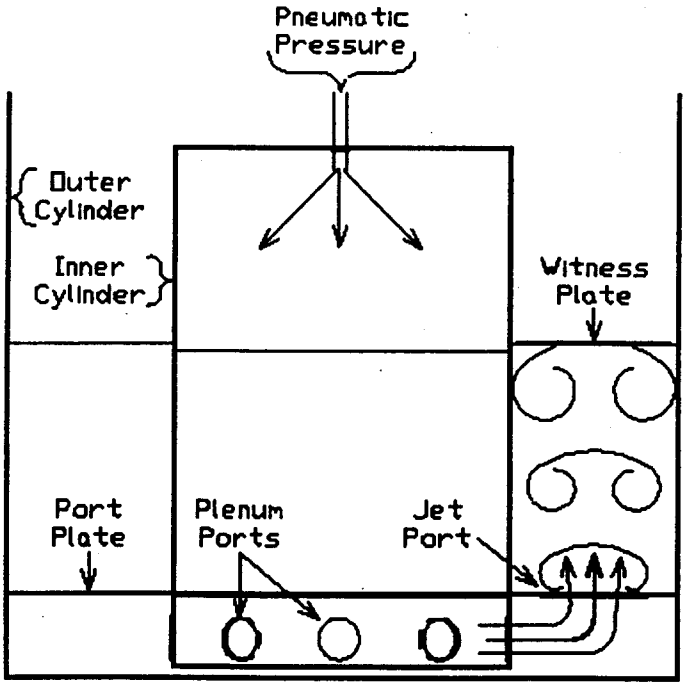

New Mexico

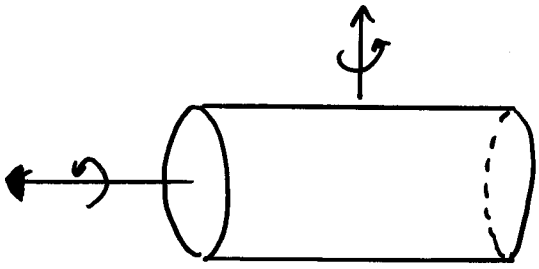

Meudon

Conclusions

- Many experiments in preparation
- Kinematic calculations are in acceptable agreement with experiments
- Saturation: laminar theories exist. Can they be transfered to the turbulent state ?
- Dynamics: few observations

Summary

Riga dynamo
(helix + return flow)

- high aspect ratio
- fluid volume separated into 3 regions
- design of propeller shape

Karlsruhe dynamo
(array of helices)

- very constrained velocity field
- separation of scales

"Ampère"
Atlanta → Maryland
Madison

- flow completely free to adjust to magnetic field
- more difficult to design (velocity profile, eddy diffusivity)